Pak. J. Chem., Vol. 1 (4), 2011

ISSN (Print): 2220-2625
ISSN (Online): 2222-307X

In the Honor of International Year of Chemistry

PAKISTAN JOURNAL OF

CHEMISTRY

An International Journal

Issue: December, 2011

Pak. J. Chem.

Chem Publishers

Editorial Board

Subscribe

- Published by the Executive Scientific Community of Pakistan
- Printed at Chem. Publishers**,** 1-K/II, Ansari Mansion, Near Chawla Market, Commercial Area Nazimabad #1, Karachi.
- Copies Available from **Chief Editor,** Pakistan Journal of Chemistry, Department of Chemistry, University of Karachi, 75270

- Subscription (National)
  - Personal → Rs. 2,000 / Volume
  - Institutional → Rs. 6,000 / Volume
  - Issue → Rs. 600 / Issue
- Subscription (International)
  - Personal → 100$ (USD) / Volume
  - Institutional → 300$ (USD) / Volume
  - Issue → 30$ (USD) / Issue

Pak. J. Chem. 1(4):148-154, 2011 Full Paper
ISSN (Print): 2220-2625
ISSN (Online): 2222-307X

Fabrication and Characterization of Metallic Copper and Copper Oxide Nanoflowers

*H. S. Virk
Nanotechnology Laboratory,DAV Institute of Engineering and Technology (DAVIET)
Kabir Nagar, Jallandhar-144008, India
Email: *hardevsingh.virk@gmail.com

ABSTRACT
Copper nanoflowers have been fabricated using two different techniques;electro-deposition of copper in polymer and anodic alumina templates, and cytyltrimethal ammonium bromide (CTAB)-assisted hydrothermal method. Scanning Electron Microscope (SEM) images record some interesting morphologies of metallic copper nanoflowers. Field Emission Scanning Electron Microscope (FESEM) has been used to determine morphology and composition of copper oxide nanoflowers. X-ray diffraction (XRD) pattern reveals the monoclinic phase of CuO in the crystallographic structure of copper oxide nanoflowers. There is an element of random artistic design of nature, rather than science, in exotic patterns of nanoflowers fabricated in our laboratory.

Keywords: nanoflowers, electrodeposition, electrolytic cell, polymer template, anodic alumina template, nanopores, hydrothermal method, morphology, nucleation rate, stiochiometry

1. INTRODUCTION
During the last decade, exhaustive reviews[1-4] have been published on metal nanostructures. A series of various nanoflowers and nanoflower-like structures have been obtained, depending on reaction conditions, such as reagents ratio, temperature and other conditions. Nanoflower structure may consist of such more simple nanostructures, as nanorods, nanowalls, or nanowires. Current and possible applications of nanoflowers as optoelectronics devices or sensors, in catalysis, and solar cells caused a definite interest in them. Nanoflowers of almost all metals have been reported in the form of elemental nanoflowers; metal oxide nanoflowers; nanoflowers of hydroxides and oxosalts; sulphide, selenide and telluride nanoflowers; nitride and phosphide nanoflowers; nanoflowers formed by organic and coordination compounds[1].
Flower-like cupric oxide (CuO) nanostructures have been prepared via cytyltrimethal ammonium bromide (CTAB)-assisted hydrothermal method[5]. CTAB is a useful surfactant that has been widely used in fabricating the nanomaterials to control the morphology. Cao et al.[6] reported CTAB-assisted hydrothermal synthesis of CuO of various morphologies such as rod-like, spheriodal, hexahedron and other irregular structures. Cupric oxide (CuO) has potential applications in many fields, such as superconductor[7], gas sensor[8], catalyst[9], magnetic storage media[10]and lithium battery[11].
Author's group[12-14] has reported fabrication and characterization of copper nanowires and some exotic patterns of polycrystalline copper recently using electrodeposition technique of template synthesis. A comprehensive investigation is planned to exploit the industrial applications of copper nanoflowers, for example, field emission properties.

2. EXPERIMENTAL
There are several different methods for fabrication of nanoflowers as reported in various reviews[1-4]. We followed two different routes for preparation of copper nanoflowers: electro-deposition technique using template synthesis and CTAB-assisted hydrothermal method.
Electro-deposition technique used in our experiment[12-14] is similar in principle to that used for the electroplating process. Commercially available polycarbonate membranes (Sterlitech, USA) of 25 mm diameter with pore density of 10^8 pores/ cm^2 and pore diameter of 100 nm were selected for this experiment. The main purpose of this experiment was to fabricate nanowires of copper. However, to our utter surprise, we failed in our mission and what we got was a blessing in disguise. We observed formation of some exotic patterns, including synthesis of nanoflowers.
A second set of experiments was completed using commercial anodic alumina membranes (AAM) (anodisc 25 made by Whatman) having an average pore diameter of 200 nm, a nominal thickness of 60 μm and a pore density of 10^9 pores/cm^2, as templates.
The electrochemical cell, fabricated in our laboratory using Perspex sheets, was washed in double distilled water. A copper rod of 0.5 cm diameter was used as a sacrificial electrode (anode). The cathode consists of copper foil attached to polymer template by an adhesive tape of good conductivity. The electrolyte used had a composition of 20 gm/100ml $CuSO_4.5H_2O$ + 25% of dilute H_2SO_4 at room temperature. The inter-electrode distance was kept 0.7 cm and a current of 2mA was applied for 10 minutes. The polymer template was dissolved in dichloromethane to liberate copper nanoflowers from the host matrix. Copper nanowires were produced generally using AAM template but in some cases, nanoflowers appeared on the periphery of template due to poor contact. The Scanning Electron

*Corresponding Author Received 1st May 2011, Accepted 22nd May 2011

Microscope (JEOL, JSM 6100) was used to record top and side views of grown nanostructures at an accelerating voltage of 20kV using different magnifications.

For hydrothermal synthesis[5], analytical grade (Loba Chemicals) copper chloride dihydrate, $CuCl_2.\ 2H_2O$, and sodium hydroxide, NaOH, were used as precursors and CTAB as surfactant. All the chemicals were directly used without further purification and de-ionized water was used for preparation of solution.

In a typical synthesis, the copper chloride solution was prepared by dissolving 0.8524g (5mmol) of $CuCl_2.2H_2O$ in 20mL de-ionized water. Subsequently, the copper chloride solution was slowly dropped into 50mL of NaOH solution ($3mol.L^{-1}$) under vigorous stirring. The blue-colored precursor was obtained. 1g of CTAB (3 mmol) was added to the blue-colored precursor and stirred vigorously for 30 min at 50 ^{0}C to ensure the complete dissolution of CTAB. This reaction solution was then transferred to a 50 mL Teflon-lined stainless steel autoclave and heated at 150 ^{0}C for 12 h in an electric oven. After reaction, autoclave was allowed to cool to room temperature. The resulting black precipitate was centrifuged and washed thoroughly with de-ionized water and ethanol. Then the precipitate was dried in drying oven at 50 ^{0}C for 24 h. Finally, the reaction products were calcined in a furnace at 500 ^{0}C for 2h in an ambient air atmosphere.

3. RESULTS AND DISCUSSION

There is as yet no specific theory to explain exotic patterns developed during electro-deposition of copper in anodic alumina or polymer templates. A speculative explanation[15] is provided on the basis of over-deposition. During the growth of copper nanowires in the template pores, the current remains nearly stable until the wires arrive at the template surface. If the electro-deposition process is not stopped at this stage, the current keeps on rising very gradually leading to over-deposition of copper. The exotic patterns in the form of micro-flowers having their petals in nanometer dimension, copper buds leading to mushroom effect and double pyramid shaped copper crystals have been observed in our investigations[12-14]. It has also been reported[16] that over-deposition of copper in polymer templates may lead to formation of metallic micro-rose having petals in nanometer dimensions. Flower- like morphology of metal over-deposits has been attributed to the changes in hydrodynamic conditions due to excessive hydrogen evolution during electro-deposition process[16].

During our recent experiments, we observed that the growth of nanoflowers depends upon two factors: cathode over-potential and conductivity of the cathode surface. If the conducting film is used for the cathode surface, Cu ions will tend to deposit into nanochannels of polymer template, otherwise they tend to grow laterally on the cathode surface. The deposition of copper takes place only when the potential of the cathode is lower than the equilibrium electrode potential of the electrolytic cell; hence, a certain magnitude of cathode over-potential is necessary. The relationship between the over-potentials and the nucleation rates was given by Erday-Gruz and Volmer[17]as follows:

$$N = a\ \mathrm{e}^{-b/\eta_k^2} \quad \textbf{(1)}$$

Where N is the nucleation rate; η_k is the cathode over-potential; and a and b are constants. It can be seen that the higher the over-potential, the higher the nucleation rates of growth. At a certain optimum over-potential, nanoflower fabrication occurs.

SEM micrographs of copper nanoflowers fabricated using polymer templates are shown (Figs. 1-3). Figure 1 shows the deposition of copper in the form of flower petals. Figure 2 depicts two different shapes of copper nanoflowers. Figure 3 represents lily-like botanical plants of copper metal grown on the cathode surface. The beauty of these experiments is that no identical patterns are produced on repeating the experiment.

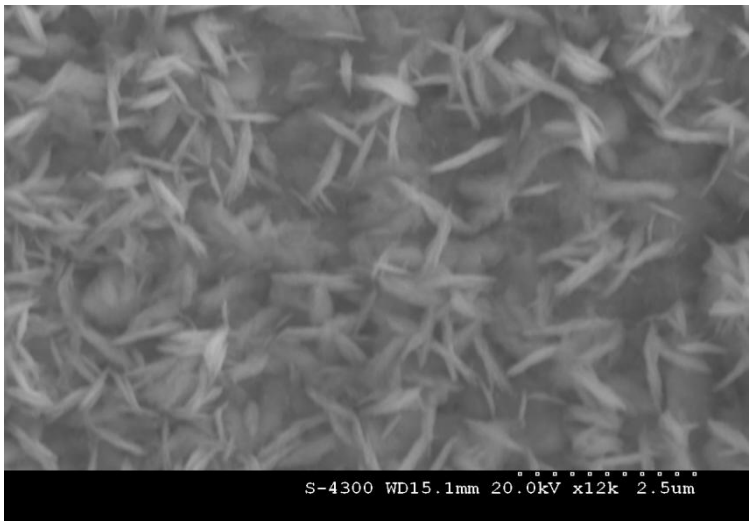

Fig-1: SEM micrograph of copper nanoflower petals grown in polymer template

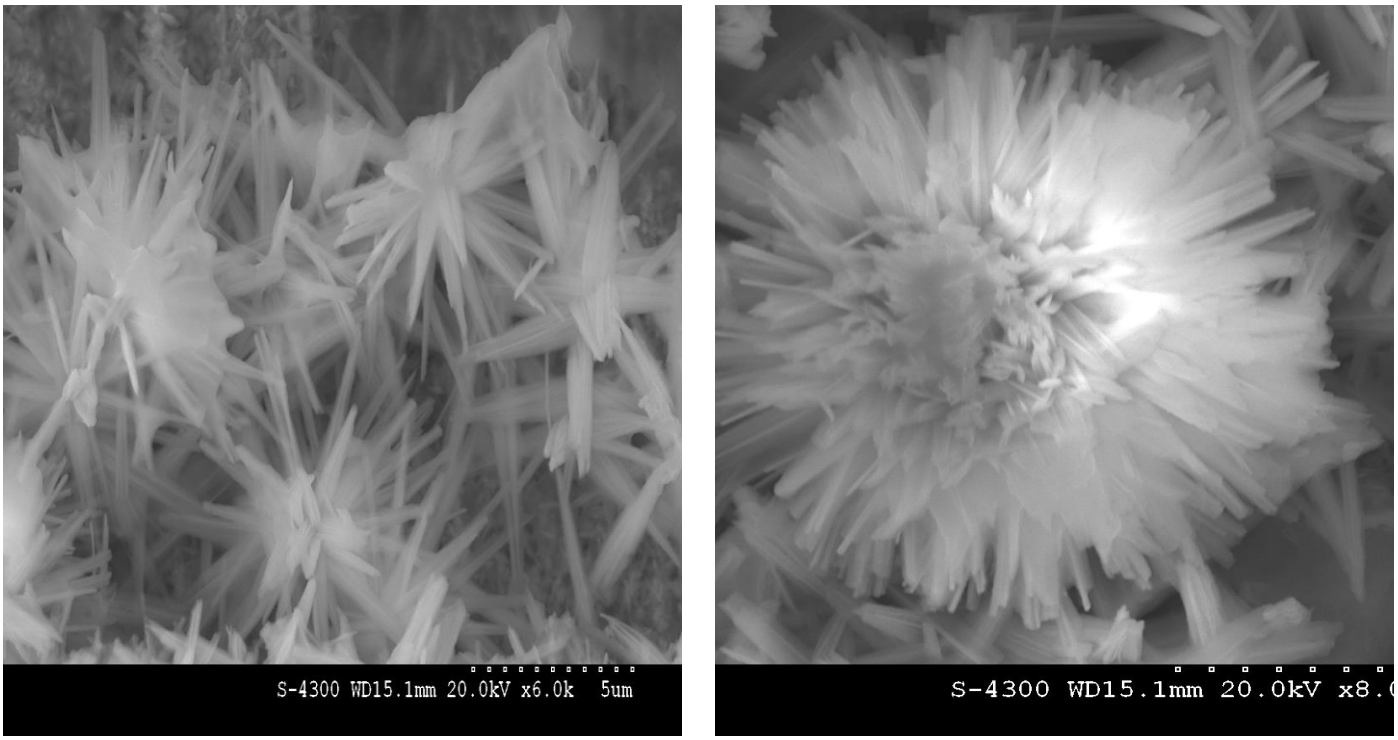

Fig-2(a,b): SEM micrographs of copper nanoflowers grown in polymer template

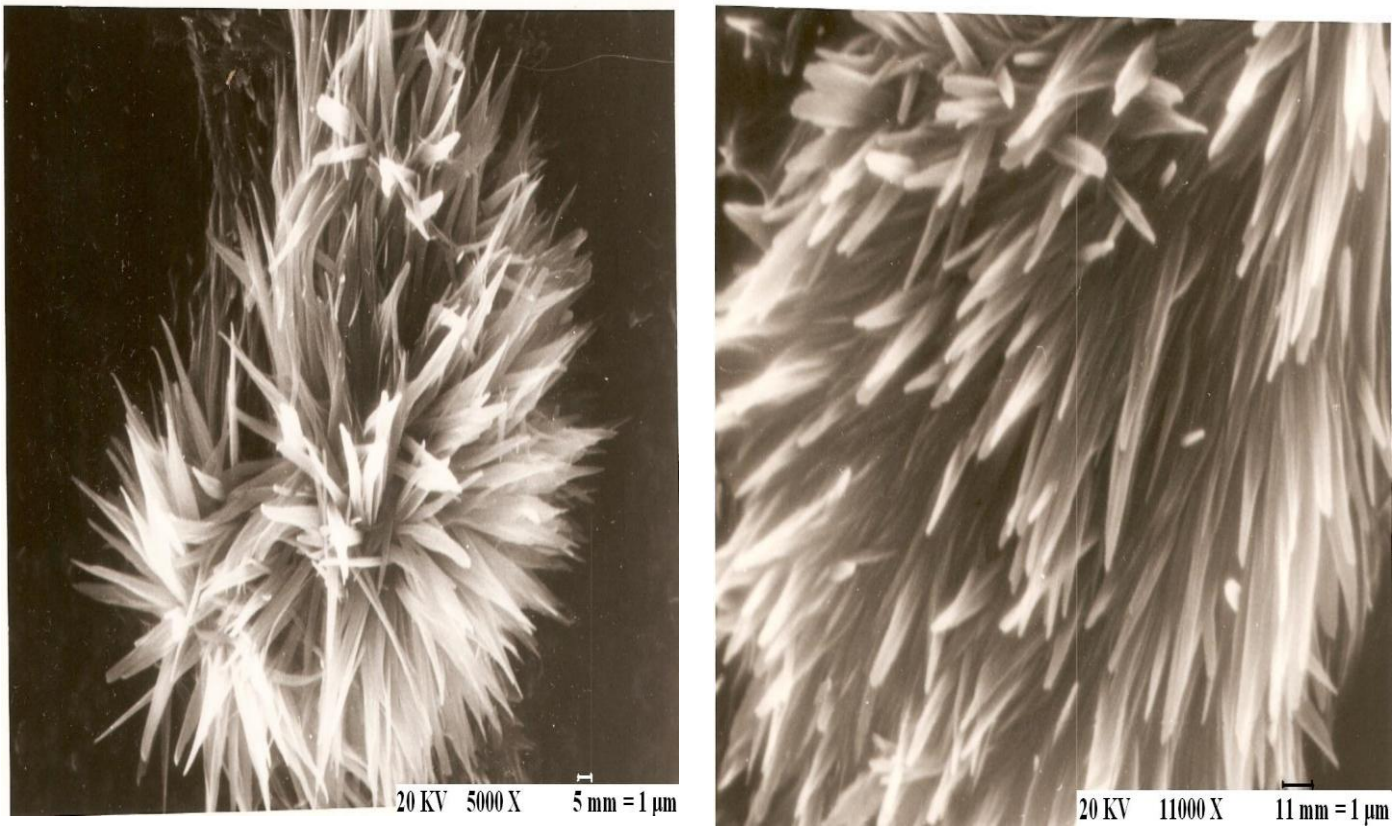

Fig-3(a,b): SEM micrograph of lily-like copper plants grown in polymer template

In case of anodic alumina template, copper nanowires[12] were grown in central region and nanoflowers in peripheral zone (Fig. 4). It shows differential deposition of copper on the cathode surface. It is difficult to determine the exact conditions under which nanoflowers are synthesized along with nanowires. Our investigations reveal that chance plays a predominant role in growth of nanoflowers. The most disturbing feature of our study is that different types of nanostructures are created under similar experimental conditions. There is an element of random artistic design in nanoflowers fabricated in our laboratory. However, there is one satisfaction that all these exotic patterns find some analogue in nature.

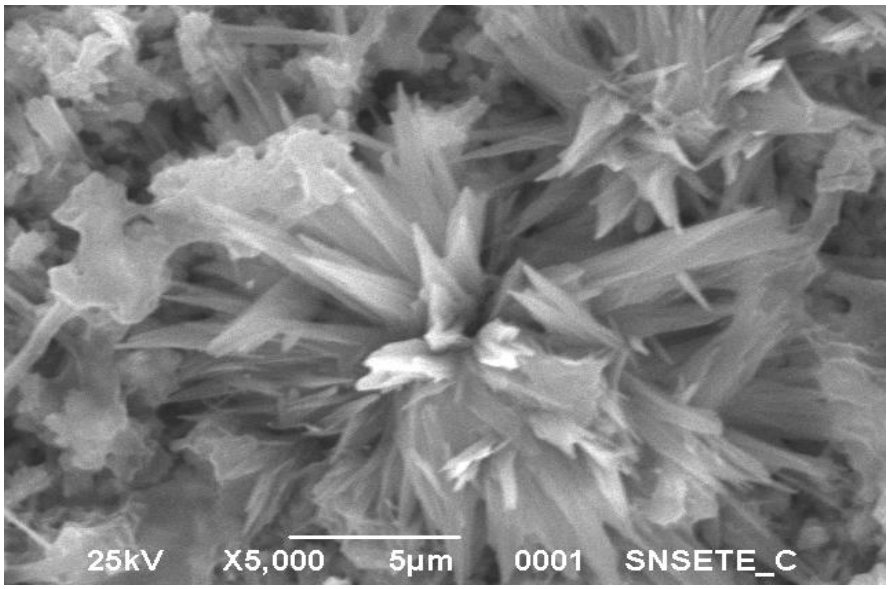

Fig-4: SEM micrograph of copper nanoflowers grown in anodic alumina template

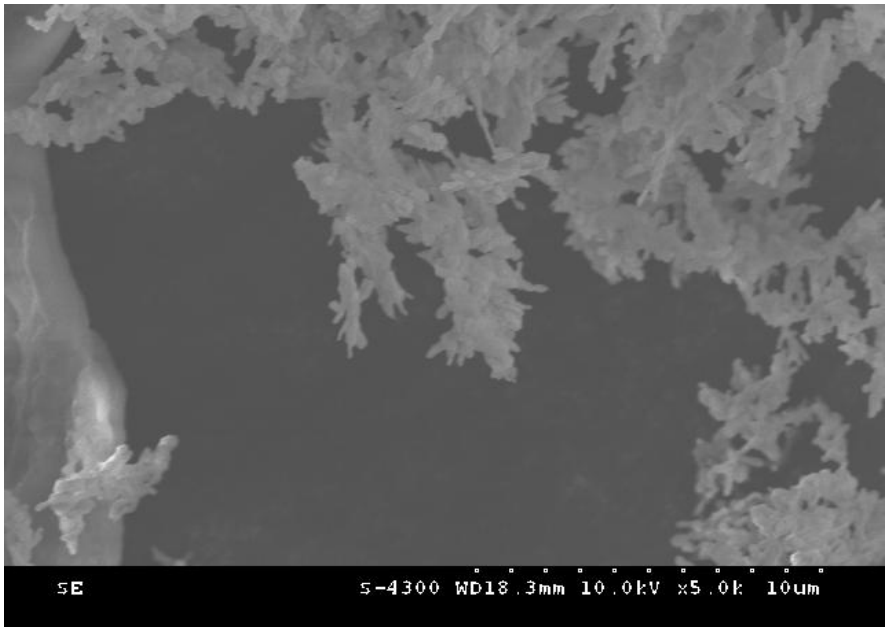

Fig-5: FESEM micrograph of CuO nanoflowers prepared by hydrothermal method

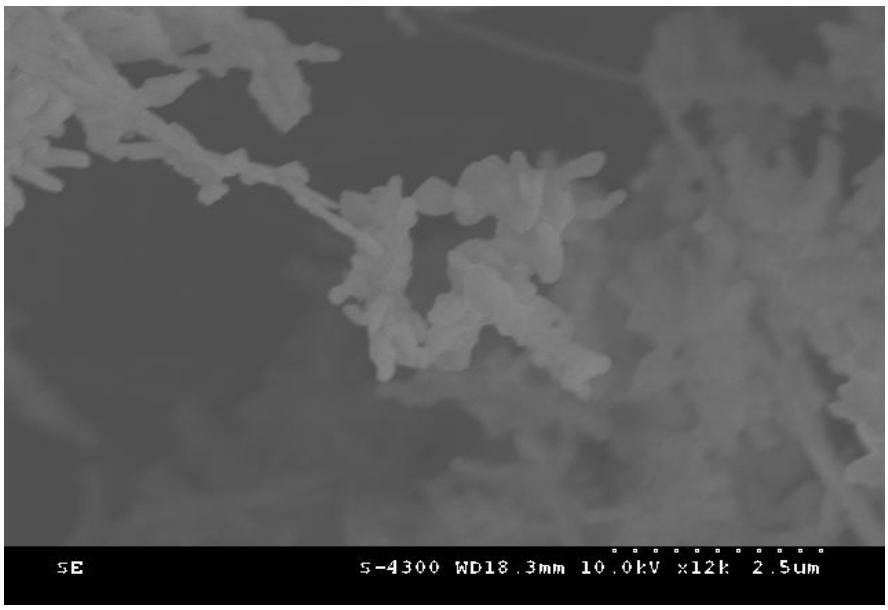

Fig-6: FESEM image depicting shape of CuO nanoflower by hydrothermal method

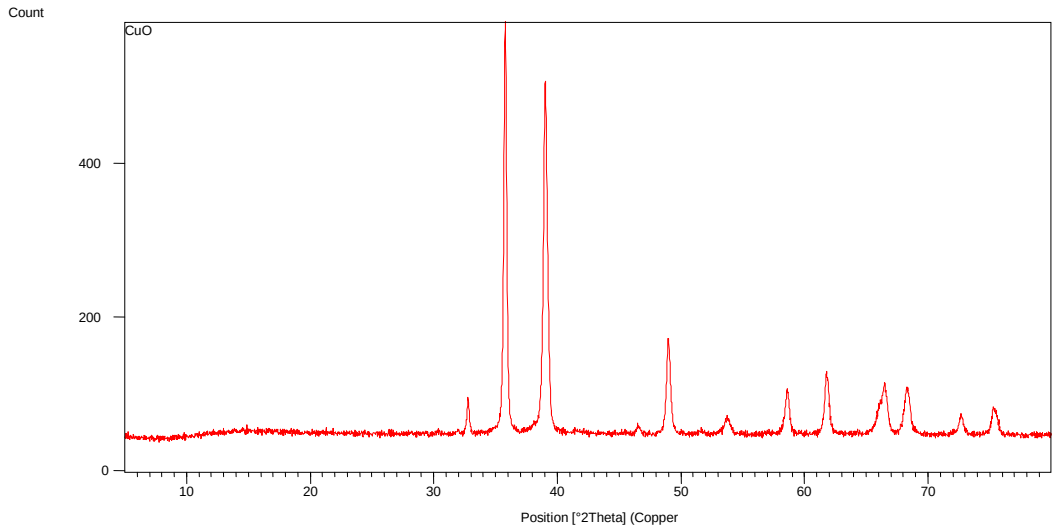

Fig-7: XRD spectrum of monoclinic copper oxide nanoflowers

\

Table-1: XRD spectrum peaks data of CuO nanoflowers

Pos. [°2Th.]	FWHM [°2Th.]	d-spacing [Å]	Rel. Int. [%]	Area [cts*°2Th.]
32.7906	0.1338	2.73127	8.01	55.93
35.8066	0.2509	2.50784	100.00	1309.41
38.9983	0.1673	2.30963	83.89	732.34
46.5518	0.2676	1.95095	1.79	24.99
48.9563	0.1506	1.86061	22.75	178.74
53.7459	0.2342	1.70556	4.34	53.09
58.6036	0.3011	1.57524	10.74	168.78
61.7668	0.2007	1.50195	14.27	149.44
66.4776	0.2007	1.40649	12.33	129.17
68.2783	0.1673	1.37372	10.87	94.87
72.6435	0.3011	1.30156	4.59	72.17
75.2766	0.1632	1.26139	6.83	78.61

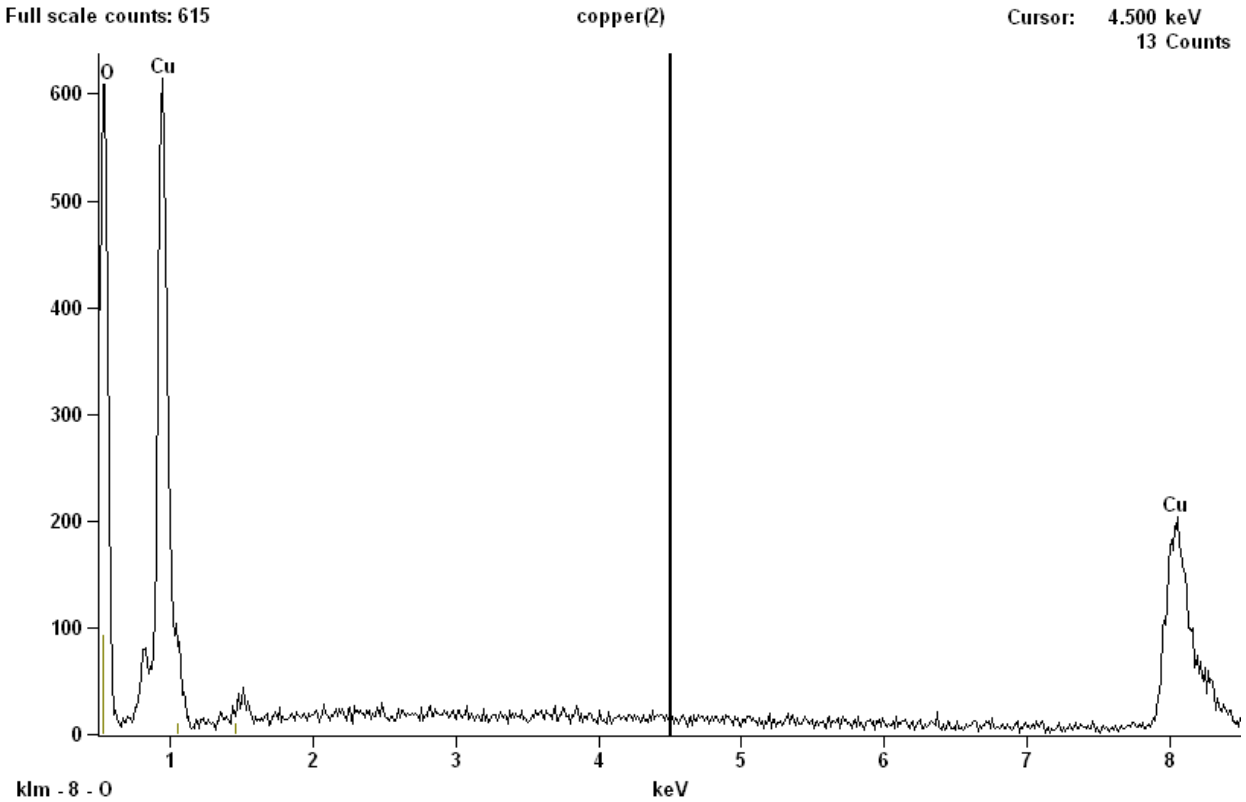

Fig-8: EDX spectrum of copper oxide nanoflowers prepared by hydrothermal method

Table- 2: Quantitative results for copper oxide nanoflowers composition

ElementLine	*Weight %*	*Weight %Error*	*Atom %*	*Atom %Error*
O K	33.60	+/- 0.73	66.77	+/- 1.44
Cu K	66.40	+/- 3.31	33.23	+/- 1.66
Total	100.00		100.00	

FESEM micrographs (Figs. 5-6) show CTAB-assisted hydrothermal synthesis of CuO nanoflowers.The explanation for CTAB-assisted hydrothermal method of CuO flowers fabrication is given by Zou et al[5]. According to the literature survey, the formation mechanisms of the flower-like CuO nanostructures were different when different preparation methods were used. Yu et al.[18] prepared the flower-like CuO nanostructures by reaction between a Cu plate and a KOH solution at room temperature and demonstrated their field emission properties. They speculated that the nanoflower was a representative morphology of spherulite formed by radiating growth from a center or a number of centers and the $[Cu(OH)_4]^{2-}$ complexes played a key role in the growth of nanoflowers. Zhu et al.[19] obtained the flower-like CuO nanostructures composed of many interconnected needle-like crystallites by hydrolyzing of $Cu(OAc)_2$ solution without any surfactants. Teng et al.[20] synthesized the flower-like CuO nanostructures by hydrothermal process using copper threads as precursor. They investigated the influences of hydrothermal temperature and hydrothermal time on the nanostructures and reported that the formation of the flower-like structure was controlled not only by the growth thermodynamics, but also by the growth kinetics.

The crystallographic structure of copper oxide nanoflowers was investigated by X-ray diffraction analysis (XRD). The typical XRD spectrum shows 12 peaks with two major peaks at $2\theta = 35.8066$ and 38.9983, corresponding to Miller indices (111) and (200). All the peaks are compared with the standard XRD spectrum[21] (AMCSD Card Number: 99-101-0934 of American Mineralogist Crystal Structure Database) and a perfect matching exists between the two spectra. In comparison with standard XRD spectrum, the main peak at $2\theta = 35.8066$ can be indexed to characteristic diffraction of monoclinic phase of CuO with cell parameters (a=0.4653 nm, b= 0.3410 nm, c= 0.5108 nm). The Miller indices of all the peaks in XRD spectrum are represented by (110), (111), (200), (201), (202), (112), (020), (113), (022), (220), (311) and (222).

Energy dispersive X-ray analysis (EDX) of CuO nanoflowers was performed using the FESEM facility of Central Scientific Instruments Organization (CSIO), Chandigarh to determine their chemical composition and stiochiometry. The spectrum (Fig. 8) reveals 3 major peaks: two peaks of copper and one peak of oxygen. Table 2 reveals that the chemical composition of nanoflowers by weight percent and atomic percent are reciprocal. EDX spectrum reveals also the chemical purity of CuO nanoflowers as other trace impurities are found to be absent.

4. CONCLUSIONS

Template synthesis is an elegant method for fabrication of copper nanoflowers, using anodic alumina or polymer templates. Over-deposition plays sterling role in the growth of exotic patterns of copper. CuO nanoflowers exhibit monoclinic phase and polycrystalline nature. No scientific theory is yet available to explain their exact nature. It has been discovered that nanoflowers have great potential for possible applications in nanotechnology. CuO nanoflowers have been exploited as sensor for hydrogen peroxide (H_2O_2)[22] and hydrazine[23], as well as for optical[24] and field emission properties[18].

5. ACKNOWLEDGEMENTS

The author is grateful to Shree C.L. Kochher, Regional Director, DAV Institute of Engineering & Technology, Jalandhar and DAV Colleges Managing Committee, New Delhi for providing research grant to set up Research Centre and Nanotechnology Laboratory in Jalandhar. FESEM analysis was carried out at CSIO, Chandigarh. Author wishes to record his appreciation to Dr Pawan Kapur, Director CSIO, Chandigarh and Dr Lalit M. Bharadwaj, Head Nanotechnology Group at CSIO for providing research facilities. Dr Inderpreet Kaur and her research team also deserve my appreciation for rendering all possible help during characterization. Mr. Mohinder Singh and Jagtar Singh at SAIF, Punjab University, Chandigarh provided all help in SEM and XRD analysis of samples, respectively, whenever I approached them. Special thanks are due to my research assistants for help in preparation of samples.

6. REFERENCES

1. Kharisov, B.I., Recent Patents on Nanotechnology, **(2008)**2(3):190-200.
2. Kharissova, O.V., Kharisov, B.I., Recent Patents on Nanotechnology, **(2008)** 2(2): 103-119.
3. Kharissova, O.V.,Kharisov, B.I., Garcia, T.H., Mendez, U.O.,Synthesis and Reactivity in Inorganic, Metal-Organic and Nano-Metal Chemistry, **(2009)**39:662-684.
4. Kharisov, B.I. and Kharissova, O.V., Ind. Eng. Chem. Res.,**(2010)**49:11142-11160.
5. Zou, Y., Li, Y., Zhang, N., Li, J., Adv. Mater. Res., **(2011)**152-153:909-914.Kharissova, O.V.,
6. Cao, M.H., Hu, C.W.,Wang, Y.H.,Guo, Y.H.,Guo, C.X., Wang, E.B., Chem. Comm.,**(2003)**15:1884-1885.

7. Schon, J.H.,Dorget, M.,Beuran, F.C.,Zu, X.Z.,Arushanov, E.,Cavellin, C.D.,Lagues, M., Nature,**(2001)**414: 434-436.
8. Tamaki, J.,Shimanoc, K., Yamada, Y., Yamamoto, Y., Miura, N.,Yamazoe, N.,Sensors& Actuators B,**(1998)**49: 121-130.
9. Reitz, J.B., Solomon, E.I., J. Am. Chem. Soc., **(1998)**120: 11467-11478.
10. Ziolo, J.,Borsa, F., Corti, M.,Rigamonti, A.,Parmigiani, F., J. Appl. Phys.,**(1990)** 67:5864-5866.
11. Gao, X.P.,Bao, J.L., Pan, G.L., Zhu, H.Y., Huang,P.X.,.Wu, F., Song, D.Y., J. Phys.Chem.B,**(2004)**108: 5547-5551.
12. Virk, H.S.,Balouria, V., Kishore, K., J. Nano Res.,**(2010)**10: 63-67.
13. Virk, H.S.,J.NanoSci.NanoEngg. & Applications, **(2010)**1(1):1-14.
14. Virk, H.S., Nano Trends, **(2010)**9(1):1-9.
15. Gao, T.,Meng, G., Wang, Y., Sun, S., Zhang, L.,J. Physics: Condensed Matter, **(2002)**14:355-363.
16. Kumar, S., Kumar, V., Sharma, M.L.,Chakarvarti, S.K.,Superlattices and Microstructures,**(2008)**43: 324-329.
17. Erday-Gruz, T.,Volmer, M., Z. Phys. Chem. A, **(1930)**150: 203.
18. Yu, L.G., Zhang, G.M., Wu, Y., Bai, X., Guo, D.Z., J. Cryst. Growth, **(2008)**310:3125-3130.
19. Zhu, J.W., Bi, H.P., Wang, Y.P., Wang, X., Yang, X.J., Lu, L.D., Mater. Lett., **(2007)**61:5236 -5238.
20. Teng, F., Yao, W.Q.,Zheng, Y.F., Ma, Y.T.,Teng, Y.,Xu, T.G., Liang, S.H., Zhu,Y.F., Sensors &.Actuators B,**(2008)**134: 761-768.
21. Downs, R.T., Hall-Wallace, M., American Mineralogist,**(2003)**88: 247-250.
22. Gu, A., Wang, G., Zhang, X., Fang, B., Bull. Material Sci., **(2010)**33(1): 17-20.
23. Zhang, X., Gu, A., Wang, G., Wang, W., Wu, H., Fang, B., Chem. Letters, **(2009)**38(5): 466-467.
24. Luo, Y., Xia, X., Ren, Q., Li, S., Li, J., Jia, Z., Dianzi Yuanjian Yu Cailiao (Chinese), **(2007)**26(2): 11-13.

Pak. J. Chem. 1(4):155-160, 2011 Full Paper
ISSN (Print): 2220-2625
ISSN (Online): 2222-307X

Measurements of Natural Radiation in soil of the College of Education, University of Kufa, Al-najaf Al-ashraf, Iraq

A. K. Hasan, *H. N. Majeed and S. A. Hassan
Education College of girls, Kufa University, Al- Najaf AL- Ashraf, Iraq.
Email: alikh_hasan@yahoo.com, *heiyam_najy@yahoo.com, saad_heswa@hotmail.com

ABSTRACT
The natural radiation of soil samples in the education college for girls which is located in kufa university in Al-Najaf Al-Ashraf govern mate have been studied . A total of 10 Soil samples were collected randomly in October 2010 then kept aside for about 4 week to ensure the equilibrium has been reached between ^{226} Ra and its decay products of short half –life and ^{228}Ra and its decay products before they were taken for gamma spectrometric analysis. The obtained values of the activity concentrations (Bq.kg^{-1}) were determined for the radionuclides ^{238}U, ^{226}Ra, ^{232}Th ,^{228}Ra , and ^{40}K. The presented results of the contents of radionuclides in soil samples showed the minimum activity concentration 4.48±0.8Bq kg^{-1} of ^{226}Ra was determined in the soil sample No. 9, while the maximum value of 49.89±10.08 Bq kg^{-1} was found in the soil from the sample No. 2. The activity concentrations of ^{232}Th were in the range 0.87±0.2 Bq kg^{-1} to 11.53±2.5 Bq kg^{-1} with a minimum value for the sample No. 1 and a maximum for the sample No. 8. The ^{40}K concentrations are disbursed as minimum value 34.54±6.7 Bq kg^{-1} in sample No.1 and maximum value 236.78±93.5 Bq kg^{-1} in sample No. 6. The highest annual effective dose rate was found to be 139.88 (μSv/y) while the world average annual effective dose equivalent is 460 (μSv/y). The corresponding gamma radiation hazard indices ,annual effective dose and gamma activity concentration index (Iγr) were below those of the limit considered acceptable.

Keywords: Radioactivity Concentration, Gamma spectrometry, soil.

1. INTRODUCTION:
Natural Background radiation consists of three primary types: Terrestrial Radiation Primordial, cosmogenic and an thropogenic, Primordial radionuclides are present in the earth's crust and found throughout the environment. Cosmogenic radionuclide's are produced when cosmic radiation interacts with elements present in the atmosphere and are deposited through both wet and dry deposition. Anthropogenic sources of radiation result from human activities, but are considered background because their presence is ubiquitous.[1-3]

1.1 *Terrestrial Radiation*
When the earth was formed four billion years ago, it contained many radioactive isotopes. Since then, all short lived radionuclides have decayed. Only those radionuclides with very long half lives (100 million years or more) remain, along with the radionuclides formed from the decay of the long lived radionuclides. These naturally-occurring radionuclides include isotopes of uranium and thorium and their decay products, such as radon. The presence of these radionuclides in the ground leads to both external gamma ray exposure and internal exposure from inhalation of radon.

1.2 *Soil*
Natural radioactive material in rocks and soil account for about 29 mrem or 8% of the radiation dose a person typically receives in a year from all sources (natural and manmade). The earth's crust contains small amounts of uranium, thorium, and radium as well as radioactive isotopes of several elements including potassium. The radiation dose comes from the gamma rays which are emitted from the rocks, soil, and some building materials (such as bricks and concrete)[1-7].

Uranium, radium, and thorium occur in three natural decay series, headed by uranium-238, thorium-232, and uranium-235, respectively. In nature, the radionuclides in these three series are approximately in a state of secular equilibrium, in which the activities of all radionuclides within each series are nearly equal. Two conditions are necessary for secular equilibrium. First, the parent radionuclide must have a half-life much longer than that of any other radionuclide in the series. Second, a sufficiently long period of time must have elapsed, for example ten half-lives of the decay product having the longest half-life, to allow for in growth of the decay products Under secular equilibrium, the activity of the parent radionuclide undergoes no appreciable changes during many half lives of its decay products.[5]

2. EXPERIMENTAL PROCEDURES
A total of 10 Soil samples were collected randomly in October 2010 , from the education college area which located in Al-Najaf AL-Ashraf city as shown in fig.(1), then dried at about 200 C^{o} for 8 hour to remove any moist .The sample were crushed to fine grain size and sieved in order to homogenize it and remove big size .The powdered samples were packed in a marinelli beaker , one kilogram from each sample and sealed tightly cap kept aside for about 4 week to ensure the equilibrium has been reached between ^{226} Ra and its decay products of short half –life and ^{228}Ra and its decay products before they were taken for gamma spectrometric analysis .

Gamma spectrometer with scintillation detector 2"× 2" inch NaI(Tl) from SPECTRUM TECHNIQUES, INC.USA .The detector was calibrated using seven radionuclides with eight γ-ray lines emitted ranged from 122.06 to

*Corresponding Author Received 11th June 2011, Accepted 5th July 2011

1332.539 keV , table (1)[8-10], which has been done for calculation the efficiency calibration fig.(2)The detector was surrounded by a lead shield to reduce the background of the system.

The activity of a specific radionuclide with a gamma energy transition could be expressed using the following equation[11-13].

$$A_{Ei} = \frac{N_{Ei}}{\varepsilon_E . t . \gamma_d M} [Bq.kgm^{-1}] \ldots\ldots\ldots\ldots (1)$$

Where A_{Ei} the activity concentration of nuclide i based on energy E, N_{Ei} the net peak area for peak at energy E , ε_E the detector efficiency at energy E, t the live time , γ_d the branching ratio for energy E of this nuclide, and M the mass of the measured sample in kg.

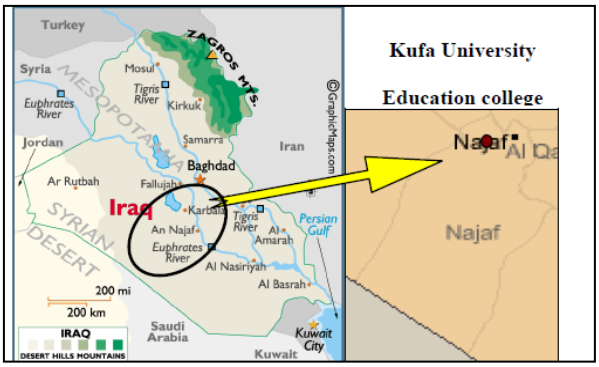

Fig-1: Map of Alnajaf Alashraf city wehre the education college surveyed during the present investigations

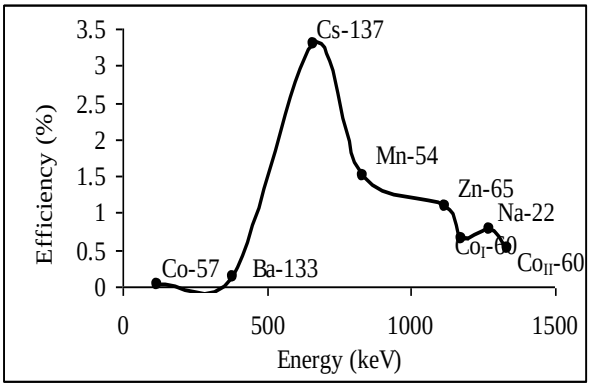

Fig-2: Full energy peak efficiency as a function of gamma ray energy for NaI(Tl) detector.

We can get the relative uncertainties of input value by[2].

$$\frac{u^2(A)}{A^2} = \frac{u^2(N)}{(N)^2} + \frac{u^2(t_c)}{(t_c^2)} + \frac{u^2 I_\gamma(E_\gamma)}{I^2{}_\gamma(E_\gamma)} + \frac{u^2\varepsilon(E_\gamma)}{\varepsilon^2(E_\gamma)} + \frac{u^2(M)}{M^2} .....(2)$$

Where $\frac{u^2(N)}{(N)^2}$ from spectra evaluation

Where $u^2(N)$ is called variance and $u(N)$ is the standard uncertainty, $\frac{u(t_c)}{(t_c)} \langle 10^{-6}$ neglected, $\frac{uI_\gamma(E_\gamma)}{I_\gamma(E_\gamma)}$ from table of intensity of gamma ray [9-11] , $\frac{u\varepsilon(E_\gamma)}{\varepsilon(E_\gamma)} = 2.5\%$ and $\frac{u(M)}{M} = 1-2\%$

We can use equation (2) to get the standard uncertainties for activity of soil samples or any environmental samples[2]

Table-1: Radionuclide used for efficiency calibration[8-10]

Nuclides	Energy (Kev)	γ_d	$t_{1/2}$
Na-22	1274.537	0.99940	2.6y
Mn-54	834.838	0.999746	312.3d
Co_I-60	1173.228	0.9985	5.27y
Co_{II}-60	1332.492	0.999826	5.27y
Zn-65	1115.539	0.5060	245d
Cs-137	661.657	0.8499	30.2y
Ba-133	356.0129	0.6205	10.5y
Co-57	122.06	0.8551	271.8d

The activity concentrations of the ^{232}Th and ^{238}U and their decay products ^{228}Ra and ^{226}Ra , were determined by the γ-ray transitions to measure the nuclides in the series[8-10,14] are as follows:

1) ^{234m}Pa (1001.03 keV) for ^{238}U.
2) ^{214}Bi (609.31, 1120.3 and 1764.49 keV), for ^{226}Ra.
3) ^{212}Bi (727.3 keV) for the ^{232}Th series.
4) ^{228}Ac (338.32, 463.1, 911.20 and 968.97 keV) for radium- ^{228}Ra
5) ^{40}K (1460.82)keV

2.1 *Radium equivalent activity (Ra_{eq})*

Distribution of ^{226}Ra, ^{232}Th and ^{40}K in environment is not uniform, so that with respect to exposure to radiation, the radioactivity has been defined in terms of radium equivalent activity (Ra_{eq}) in Bq.kg[-16,12,13].

$$Ra_{eq} = A_{Ra} + 1.43A_{Th} + 0.077A_K \ldots.(3)$$

Where A_{Ra} , A_{Th} and A_K are specific activity concentration in Bq.kg^{-1} of ^{226}Ra, ^{232}Th and ^{40}K, respectively. The index is useful to compare the specific activity of materials containing different concentrations of ^{226}Ra, ^{232}Th and ^{40}K.

2.2 *Gamma Dose Rate (D)*

The total dose rate D in the air (out doors) due to uniform distribution of all the ^{226}Ra, ^{232}Th and ^{40}K in the beach soil 1 m above the ground surface was estimated by[6,12,13,15]

$$D = 0.427A_U + 0.662A_{Th} + 0.043A_K \ldots.(4)$$

Where D is the dose rate in (nGy.h^{-1}) and A_U , A_{Th} *and* A_K are the concentrations of uranium, thorium and potassium, respectively.

2.3 *Annual Effective Dose Equivalent (AEDE)*

In order to estimate the annual effective dose rate in air the conversion coefficient from absorbed dose in air to effective dose received by an adult had to be taken into consideration .This value is published in UNSCEAR (2000) of(0.7 Sv/Gy).The outdoor occupancy factor which is about (0.2) .

The annual effective dose equivalent was given by the following equation[6,12,13,15]

$$\text{AEDE}(\mu\text{Sv/y}) = \text{D(nGy/h} \times 8760\text{(h/y)} \times 0.2 \times 0.7\text{(Sv/Gy)} \times 10^{-3}$$

….(5)

2.4 *Representative level index (Iγr)*

In order to examine whether the sample meets limits of dose criteria ,Another radiation hazard index, representative level index *Iγr*, used to estimate the level of *γ*- radiation hazard associated with the radionuclides in specific investigated samples ,is defind as the following equation[6,12,13,15]

$$I_{\gamma r} = A_{Ra}/150 + A_{Th}/100 + A_K/1500 \ldots..(6)$$

The index Iγr was correlated with the annual dose due to the excess external gamma radiation caused by superficial material. Values of index I ≤1 correspond to 0.3 mSv/y, while I ≤3 correspond to 1 mSv/y. Thus, the activity concentration index should be used only as a screening tool for identifying materials which might be of concern to be used as covering material. According to this dose criterion, materials with I ≤ 3 should be avoided[15].

2.5 *External hazard index (H_{ex})*

The external hazard index (H_{ex}) was given by the following equation[6,12,13,15]

$$H_{ex} = \frac{A_{Ra}}{370} + \frac{A_{Th}}{259} + \frac{A_K}{4810} \ldots..(7)$$

2.6 *Internal hazard index (H_{in})*

The internal exposure to ^{222}Rn and its radioactive progeny is controlled by the internal hazard index (H_{in}) is given by[6,12]

$$H_{in} = \frac{A_{Ra}}{185} + \frac{A_{Th}}{259} + \frac{A_K}{4810} .....(8)$$

For the safe use of a material in the construction of dwellings, index (H_{in}) should be less than unity and the maximum value of (H_{in}) to be less than unity.

3. RESULTS AND DISCUSSION

Soil is a significant part of the human environment that provides resources for food production. It is a very dynamic ecosystem of particular importance since, once contaminate, the soil acts as a potentially long-term source of environmental contamination of food, water and air[16].

Table-2: Concentrations of radionuclide for each sample

Sample No.	^{238}U	^{226}Ra	^{232}Th	^{228}Ra	^{40}K
1	41.45±7.9	37.85±3.7	0.87±0.2	0.82±0.2	34.54±6.7
2	32.04±9.6	49.89±11.1	1.28±0.4	0.75±0.2	62.63±12.6
3	33.28±9.4	43.45±9.9	1.16±0.3	1.1±0.3	38.83±9.9
4	77.17±15.6	49.25±7.1	3.06±0.6	1.02±0.3	114.77±22.5
5	42.64±12.8	35.56±7.9	1.71±0.5	1.006±0.3	127.94±23.2
6	112.47±37.8	6.41±1.7	2.09±0.4	3.54±1.2	236.78±93.5
7	123.98±33.9	15.91±4.8	6.35±1.5	9.506±1.5	49.59±38.7
8	153.5±49.6	23.32±15.3	11.53±2.5	9.5±2	76.75±72.1
9	253.63±43.5	4.48±0.8	3.66±1.3	1.86±0.3	77.64±48.9
10	83.46±33.7	26.52±5.3	7.13±1.7	11.33±1.7	133.54±67.1
Aver.	95.36±25.4	29.27±6.8	3.88±0.9	4.04±0.8	95.305±39.5
Max.	253.63±49.6	49.89±15.3	11.53±2.5	11.33±2	236.78±93.5
Min.	32.04±7.9	4.48±0.8	0.87±0.2	0.75±0.2	34.54±6.7

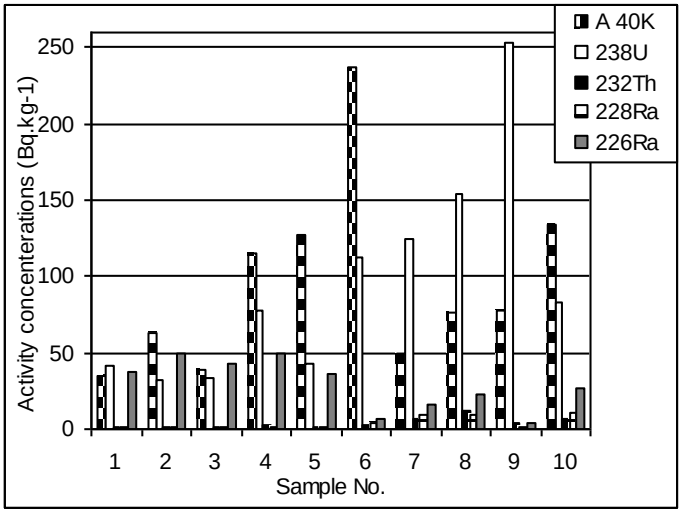

Fig-3: The specific activity of ^{238}U,^{232}Th,^{226}Ra, ^{228}Ra and ^{40}K in Bq.kg^{-1}

The obtained values of the activity concentrations (Bq.kg^{-1}) determined for the radionuclides ^{238}U, ^{226}Ra, ^{232}Th , ^{228}Ra , and ^{40}K, in the analyzed soil samples were listed in Table (2) fig.(3) , while the ^{238}U/^{226}Ra , ^{232}Th/^{228}Ra and ^{238}U/^{232}Th ratio were shown in fig (4). The presented results of the contents of radionuclides in soil samples showed. The minimum activity concentration 4.48±0.8Bq kg^{-1} of ^{226}Ra was determined in the soil sample No. 9, while the maximum value of 49.89±10.08 Bq kg–1 was found in the soil from the sample No. 2. The activity concentrations of ^{232}Th were in the range 0.87±0.2 Bq kg^{-1} to 11.53±2.5 Bq kg^{-1} with a minimum value for the sample 1 and a maximum for the sample No. 8.

The ^{40}K concentrations are disbursed as minimum value 34.54±6.7 Bq kg^{-1} in sample No. 1 and maximum value 236.78±93.5 Bq kg^{-1} in sample No. 6. The ^{238}U/^{232}Th ratio showed the low concentration of ^{232}Th series with respect to ^{238}U series .The differences were attributable to the geochemical composition and origin of soil types in this area.

All calculated Iγr, external and Internal hazard indexes were below the unity . Therefore ,the obtained values from this preliminary study were all lower than the accepted ,average worldwide value. The highest annual effective dose rate was found to be 139.88 (μSv/y) were less than the world average 460 (μSv/y)[6,12,13,15].

Table-3: Radium equivalent (Bq/kg), dose rate (nGy/h) and *AEDE (μSv/y),* for all samples

Sample No.	Ra_{eq}	D(nGy/h)	AEDE(μSv/y)
1	41.76	19.76	24.23
2	56.56	17.23	21.13
3	48.11	16.65	20.42
4	62.47	39.91	48.95
5	47.86	24.84	30.47
6	27.64	59.59	73.08
7	28.83	59.28	72.706
8	45.73	76.48	93.8
9	15.69	114.06	139.88
10	47.01	46.106	56.54
Ave.	42.17	47.39	58.12
Max.	62.47	114.06	139.88
Min.	15.69	16.65	20.42

Table-4::The external, internal ,and representative hazard indexes for all samples

Sample No.	$H_{ex}\leq 1$	$H_{in}\leq 1$	Iγr≤1
1	0.12	0.23	0.03
2	0.17	0.32	0.059
3	0.14	0.27	0.044
4	0.20	0.37	0.1139
5	0.162	0.29	0.109
6	0.13	0.2	0.202
7	0.112	0.19	0.16
8	0.18	0.307	0.229
9	0.072	0.115	0.1
10	0.182	0.309	0.23
Ave.	0.148	0.262	0.129
Max.	0.2	0.373	0.23
Min.	0.072	0.115	0.037

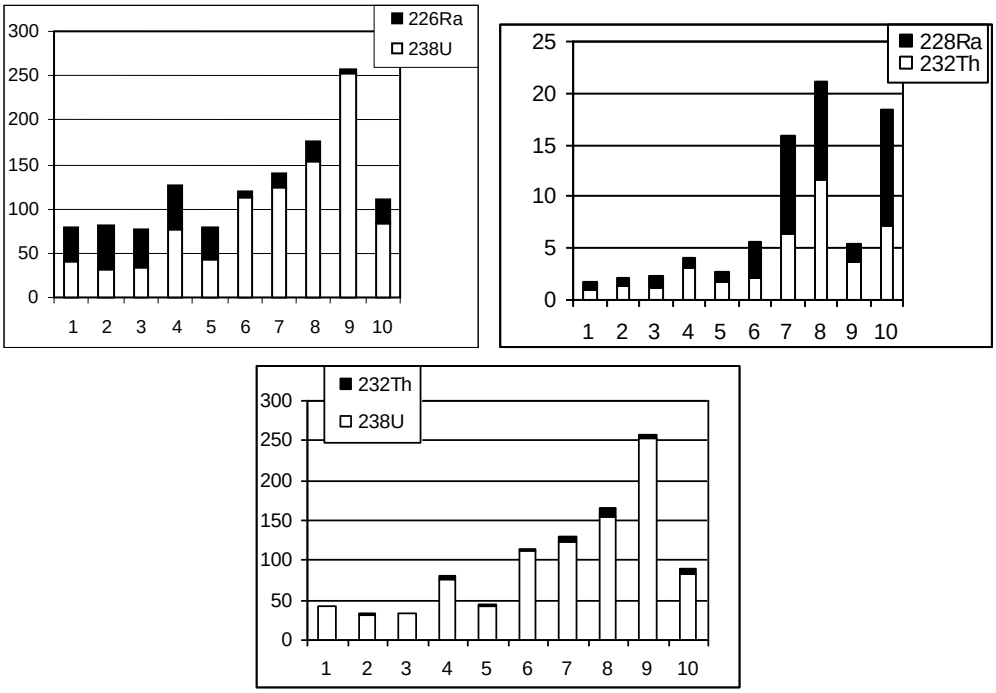

Fig-4: $^{238}U/^{226}Ra$, $^{232}Th/^{228}Ra$ and $^{238}U/^{232}Th$ ratio respectively .

4. CONCLUSION

The measured levels of the natural radiation background in the present study from the all investigated samples showed that the studied areas have normal levels of background radiation[9-11]. The corresponding gamma radiation hazard indices ,annual effective dose and gamma activity concentration index (Iγr) were below the acceptable limits.

5. REFERENCES

1. Okeyode I, Oluseye A Physics International **(2010)** 6: 1-8
2. Harb S, PhD thesis , ZSR, Hannover university, Germany **(2004)**.
3. Damon R MSc .thesis , the University of the Western Cape, Bellville **(2005).**
4. Argonne National Laboratory, Natural Decay Series: Uranium, Radium, and Thorium EVS Human Health Fact Sheet. **(2005)**.
5. Argonne National Laboratory, Potassium-40, EVS Human Health Fact Sheet. **(2005)**
6. Radenković S Alshikh V Andric V,and Miljanic S , J. Serb. Chem. Soc. **(2009)** 74 :461–470
7. Egunyinka O Olowookere C Jibirind N Babalola I and Obed R, The Pacific Journal of Science and Technology, **(2009)** 10: 742-752
8. International atomic energy agency, Update of x ray and gamma ray decay data standards for detector calibration and other applications, Volume 1, Vienna **(2007)**.
9. International atomic energy agency, Update of x ray and gamma ray decay data standards for detector calibration and other applications ,Volume 2, Vienna **(2007)**.
10. IAEA, Guidelines for radioelement mapping using gamma ray spectrometry data", Vienna **(2003)**.
11. Ebaid Y Rom. Journ. Phys. **(2010)** 55-69-74.
12. Harb S, El-Kamel A, Abd El-Mageed A and Wafaa R, Proceedings of the 3rd Environmental Physics Conference, **(2008)** 19-23 Feb. Aswan, Egypt.
13. Al-Sulaiti H ,Regan P, Bradley D, Matthews M, Santawamaitre T and Malain D IX Radiation. Physics & Protection onference, 15-19 November Nasr City - Cairo, Egypt. **(2008)**
14. Abdulla A, Aldrgazelli S and Elias M " Experimental Nuclear Physics", Iraq. **(1990)**
15. Al – Saleh F and Al-Berzan B, Journal of Nuclear and Radiation Physics **(2007)** 2,25-36.
16. AL-SAIF A, MSc. Thesis King Saud University. **(2009)**

Pak. J. Chem. 1(4):161-163, 2011 Full Paper
ISSN (Print): 2220-2625
ISSN (Online): 2222-307X

The Therapeutic role of Magnesium in different depressive syndromes of the male population comprising of different age groups

[*]N. Bano, R. Najam and [1]S. Naeem
[1 *]Assistant Professor, Faculty of Pharmacy, Jinnah University For women.
Chairperson, Professor, Department of pharmacology, Faculty of Pharmacy, University of Karachi.
Email: [*]nusratbano@hotmail.com

ABSTRACT
The basic and fundamental role of Mg as being the second most abundant intercellular cation is established in various studies. It is identified as a divalent metal cofactor in over 300 enzymatic reactions involving energy metabolism and protein and nucleic acid synthesis. The biological function is identified in neuromuscular excitability. Mg ion regulates calcium ion flow in neuronal channels, helping to regulate neuronal Nitric Oxide production[1]. Mg deficiency causes NMDA coupled Calcium channels to be biased towards opening, causing neuronal injury & neurological dysfunction, which may appear to humans as major depression. The present study confirms a reduction in the symptoms of depression found in the male population comprising of different age group by Mg treatment. CSF Mg has been found low in treatment resistant suicidal depression. Brain Mg is also low in TRD using phosphorous nuclear magnetic resonance Spectroscopy[2]. A 2009 randomized clinical trial shows that Mg therapy was an effective as TCAs in depressed diabetics. Increase in brain Mg enhances both short term synaptic facilitation and long term potentiation and improves learning and memory function[3] The present study is based on findings that male subjects diagnosed as depressed showed a marked reduction in behavioral and somatic features of the disease after administration of Magnesium supplement. Physiological and somatic anxiety was also alleviated in a certain age group which displayed recovery from Insomnia and agitation. Suicidal tendency was also negative in all age groups. This study focuses on the behavioral and somatic responses pertaining to brain biochemical changes induced by Magnesium therapy.

Keywords: Depression, magnesium, antidepressants, insomnia, guilt feeling, calcium channels ,suicidal depression, hypochondriasis

1. INTRODUCTION
The psychological and physical symptoms leading to specific behavioral and somatic features of major depression are identified and evaluated in this study for male patients comprising of three different age groups. The patients are classified as subject of either reactive/secondary depression or bipolar effective disorder. It is established that besides biological vulnerability of the disease to be inherited, a combination of genetic, psychological and environmental factors are involved in depressive disorder, later episodes of illness typically are precipitated by only mild stress.

The male patients included in the study were clinically diagnosed by DSM IV as patients of chronic pain with major depression at the stage of diagnosis ,low CSF magnesium and calcium are involved in many processes related to depression.[4] Valid studies have confirmed that hypercalcemia and hypomagnesaemia are associated with depression[5] based on the relationship of cations magnesium functions as a calcium antagonist. Serum and CSF ca/mg ratio are found to be elevated in depressed patients[6], whereas patients of chronic pain with depression identified with low levels of CSF magnesium offer considerable data bearing clinical significance. Magnesium is a natural ca channel blocker. clinically magnesium deficiency has been associated with cardiac arrthymia, hypertension, MI, stroke, anxiety, migraine, panic attacks, epilepsy, osteoporosis, immune dysfunction as well as chronic fatigue, acute musculoskeletal pain and reflex sympathetic dystrophy, all illnesses with high incidence of concomitant depression[7-10]

2. MATERIAL AND METHOD
Thirty male patients were diagnosed with depression by a positive DSM IV test for depression[11] as well as MMPI and clinical evaluation. These patients were classified in three age groups for assessment and clinical assessment of specific features such as agitation, guilt feeling, psychomotor retardation, insomnia, anxiety, weight loss and hypochondria. These patients were also subject to chronic pain with depression. The patients underwent lumbar puncture as part of an evaluation for headache or suspected meningitis and were found to demonstrate no physical or mental disorder. A low level of magnesium in the CSF was detected in all patients.

The patients underwent standard measurement of cell magnesium by magnesium load test[12] all thirty patients were found deficient in magnesium. The dietary intake of the patients were assessed during the course of study with a comprehensive food frequency questionnaire. The thirty patients were treated with a daily dose of oral Magnesium Taurate for six weeks and psychomotor and psychological symptoms were carefully monitored. The patients were divided into three categories of age group.

1) Age group 15-24 2)Age group 25-34 3)Age group 35-44

*Corresponding Author Received 8th October 2011, Accepted 23rd October 2011

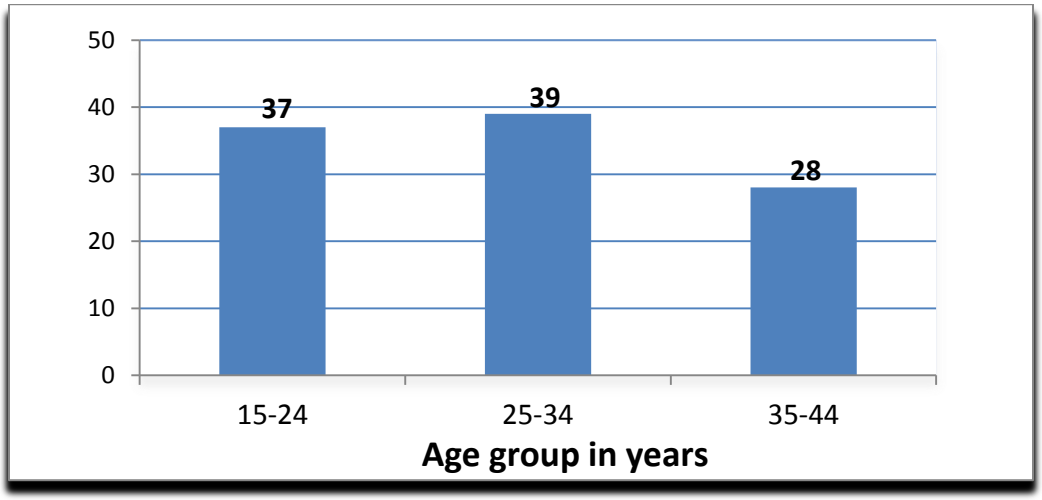

Table-1: Symptoms decreased /improvement (%) after treatment according to age

S.No.	Symptoms	Age in years		
		15-24	25-34	35-44
1.	Depressed Mood	16.7	16.7	62.5
2.	Guilt Feeling	66.7	66.7	33.3
3.	Suicidal Tendency	1.4	44.4	66.7
4.	Insomnia(early, middle, late)	20.0	40.0	0.0
5.	Work and Activities	40.0	57.1	33.3
6.	Retardation-Psychomotor	50.0	66.7	50.0
7.	Agitation	50.0	20.0	33.3
8.	Anxiety Psychological	40.0	50.0	60.0
9.	Anxiety Somatic	40.0	80.0	0.0
10.	Somatic Symptoms GI	50.0	75.0	0.0
11.	Somatic Symptoms General	0.0	0.0	0.0
12.	Sexual Dysfunction/Menstrual Disturbance	80.0	20.0	50.0
13.	Hypochondrias	0.0	25.0	0.0
14.	Weight Loss	0.0	0.0	0.0
15.	Insight	50.0	20.0	33.3

3. RESULTS AND DISCUSSION

Depressed mood was relieved in all the age groups and was markedly reduced in age group35-44 after oral magnesium intake. The group was labeled for treatment resistant depression (hereafter referred to as TRD), however the male patients exhibited marked reduction of behavioral and somatic features of the disease after administration of magnesium supplement. The response in male patients with TRD has been reported in previous studies as well[13]

Symptoms of guilt feeling were much reduced in age group 15-24 and group 25-34. Both the age groups demonstrated a better judgment of self-esteem after six weeks of magnesium therapy. It was also noted that diabetic males in each group found relief from the intense guilt feeling at early stage of magnesium supplementation. Some studies[14] show that blood glucose levels cause flushing of different minerals along with magnesium sparing calcium.

Suicidal tendency and relishing the idea of suicidal attempts was overall resolved in all the patients. Significant improvement was seen in age group 15-24 after magnesium therapy. A previous trial has shown that magnesium supplementation with varapamil reduces suicidal tendency in male patients with mania.

Insignificant relief of insomnia is observed in all age groups. Maximum improvement in work and activities was seen in age group 25-34.the erythrocytes and also plasma magnesium is shown to be associated with the intensity of depression. Blood hypomagnesaemia and CSF hypermagnesemia causes hyperexcitability in depressed people[15], further investigations are in process to show whether hypermagnesemia might be in contrast associated with psychomotor retardation as observed in depressed patients. After intake of oral magnesium supplements for six weeks psychomotor retardation was reduced in all the patients. Age group 15-24 also exhibited relief from agitation. psychological anxiety was relieved markedly in age group 35-44.whereas somatic anxiety was reduced in age group 25-34 markedly. This group

also responded to magnesium intake by showing a reduction in somatic symptoms GI. General somatic symptoms however were not relieved.

Sexual function was improved in age group 15-24. Hypochondrias was not relieved in any age group except for age group 25-34. There was no weight loss seen in any patient. Insight was improved the most in age group 15-24. the chronic pain with depression is reduced in each patient with an overall sensation of wellbeing.

4. CONCLUSION

On the basis of the study magnesium is found to alleviate the physical and psychological symptoms of depression. Magnesiumtaurate therapy at a daily dose of 450mg is also effective in TRD and can also be given with classical antidepressants for synergestic effects. Increased intake of magnesium rich food substances in patients of anxiety and depression is advised. The study of effect of magnesium therapy at different doses in depression or chronic depression with diabetes bears ample prospect and is open for study.

5. REFERENCES

1. Galburt E.A, Stoddard B.L Biochemistry 4 **(2002)** 1:13851-13860
2. Inna Slutsky, Nashat Abumaria, Long-Jun wu, Chao Huang. Enhancement of learning and memory by elevating rain magnesium.Neuron, Jan 28, **(2010)**.
3. Med Hypothesis 2010 Apr; **(2009)** 74(4):649-60.EPub Nov 27.
4. Bank CM, et.al Biol Psychiatry Feb; **(1985)** 20(2)163-71.
5. Levine J, et.al. Neuropsychobiology **(1999)** 39(2)63-70.
6. Widmer Jet.al J Affect disorder, June 8; **(1995)** 34(3);201-9.
7. Seeling MS: Magnesium Deficiency in the Pathogenesis of Disease, New York, Plenum Publishing Corporation, **(1980)**.
8. Seeling, MS: Magnesium Deficiency in Two Hypertensive Patient Groups. Southern Medical Journal **(1990)** 83:739-42.
9. Reinhart RA: Magnesium Metabolism. Arch Intern Med **(1988)** 148:2415-2420.
10. Seeling CB: Magnesium Deficiency in Two hypertensive Patient groups. Southern Medical Journal **(1990)** 83:739-742.
11. DSM IV (Diagnostic and manual of mental disorder 4rth edition, Washington. D.C: APA, **(1994)**:Copyright 1994.
12. Ryzen E, Elbaum N, Singer FR, et al: Parenteral Magnesium Tolerance Testing in the Evaluation of Magnesium Deficiency. Magnesium **(1985)** 4:137-147.
13. Eby KL. Med Hypotheses. Apr; **(2010)** 74(4):649-60. Epub (2009) Nov 27.
14. Barbagello, renick **(1994)**.
15. Widmer J, J Affect Disord. Jun 8; **(1995)** 34(3):201-9.

Pak. J. Chem. 1(4):164-167, 2011 Full Paper
ISSN (Print): 2220-2625
ISSN (Online): 2222-307X

Influence of Seed pre-treatment by UV-A and UV-C radiation on germination and growth of Mung beans

*N. Hamid and F. Jawaid
Department of Botany, University of Karachi, Karachi 75270, Pakistan
Email: neelofer_physio@yahoo.com

Abstract
The consequence of pre-treatment of UV-A (366 nm) and UV-C (254 nm) radiation on seed germination and growth of *Vigna radiata* was investigated at three different exposure period (2, 4 and 6 hours). Supplementation of UV-A enhanced the germination rate, specific leaf area, root and shoot length and dry weight than the UV-C supplemented plants.

Keywords: Dry mass; Root length; Seed Germination; Shoot length; Specific leaf area; UV-A; UV-C; *Vigna radiata.*

1. INTRODUCTION

Release of halogenated hydrocarbons (chlorofluorocarbons) and many trace gases (methane and Nitrous oxide) in the atmosphere due to numerous anthropogenic human activities resulting in the depletion of the stratospheric ozone layer [1]. Stratospheric ozone plays a very important role in defending the earth's surface from ultraviolet radiation [2]. Depletion of Stratospheric ozone is expected to increase the amount of solar ultraviolet radiation reaching the surface of earth which can damage the biological ecosystems [3]. A 10% depletion in stratospheric ozone corresponds to a 20% increase in the capability of biologically damaging UV-B, which is likely to enhance in future, if ozone destruction is not checked [4]. The UV spectrum is usually separated into three regions: the UV-C region (220- 280 nm), the UV-B region (280 - 320 nm) and the UV-A region (320 - 400 nm). UV-B radiation is the most active constituent of sunlight reaching the earth's surface as compare to UV-A[5].

Enhance in the solar UV radiation reaching the biosphere may have several effects on global plants by increasing the biological damage [6]. UV radiation induced alteration in photosynthesis, cell division and other life processes of direct importance to growth and development such as alterations in plant hormones and nucleic acids [7]. Although defensive and repair mechanisms exist to counteract the effects of increased UV radiation [8]. According to another report morphological, physiological and biochemical significance of UV radiation on vast varieties of plants system have been observed [9]. Several researchers reported the potential effects of UV-B on vegetative growth and photosynthetic activities of higher plants[10].

By means of this background, we hypothesize that seed pre-treatment by UV radiation boosted the rate of seed germination and improve vegetative growth. The present study was designed to assess the effects of pre-treatment of two UV regions i.e. UV-A (366 nm) and UV-C (254 nm) radiation on the Specific leaf area, root and shoot length and dry weight and percent germination of *Vigna radiata*, a leguminous plant.

2. EXPERIMENTAL

Mung bean (*Vigna radiata*) seeds were obtained locally. Seeds were alienated into small batches, which were stored in closed glass bottle in refrigerator at 4°C. For irradiation seeds samples were removed from the refrigerator and the seeds, still in their airtight glass bottles, were kept closed overnight to equilibrate with laboratory temperatures before irradiation. Then these seed were irradiated by UV using 022.9064 The CAMAG UV cabinet ll which comprised of the CAMAG universal UV lamp having dual wavelength 254nm (short wave) and 366nm (long wave), two light tubes 8 watt each. Seeds were exposed for 2, 4 and 6 hours at both wavelengths and non treated seeds were serving as control.

Twenty one Petri dishes of 9cm diameter each were containing two filter papers (Whatman no. 1 of 90mm thickness). The top of all Petri dishes were removed after which the dishes were divided into seven groups of three Petri dishes. Twenty seeds of each treatment (4 rows of 5 seeds) were placed in the wet filter paper. The distance between adjacent seeds was sufficient (five times greater than diameter of seeds). Petri dishes were kept in germinator at 23/18°C during course of experiment; the filter papers were humidified regularly with distilled water. The germination of seeds was followed for seven days. Number of germinated seeds was recorded after 1, 2, 3, 4, 5, 6 and 7 days and germination percentage was recorded. After germination seven days old seedling were transplanted in plastic pots (12cm diameter and 15cm height) contains 1.5 Kg of soil which was provided with 50mg of NPK fertilizer. Different parameters of growth like shoot and root length, dry mass and specific leaf area were calculating after 10 days interval up to 60 days. Shoot and root length and specific leaf area were carefully calculated and observations were recorded in Cm and Cm^{-2}.gm respectively. Dry mass (gm) was determined after drying in an oven at 70°C for 48 hours.

*Corresponding Author Received 24th September 2011, Accepted 13th October 2011

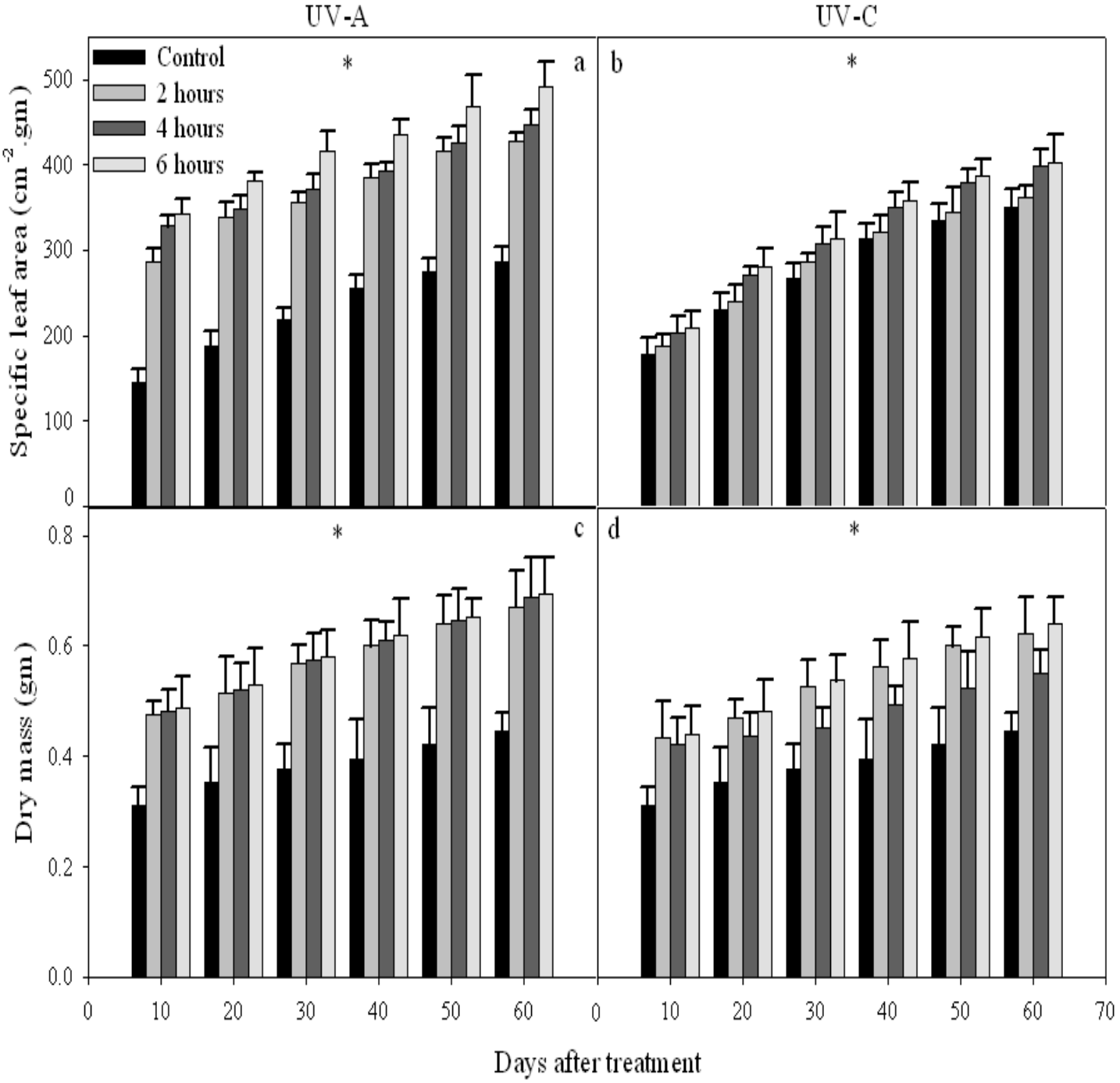

Fig-1: Effect of UV-A and UV-C enhanced radiation on specific leaf area (a, b) and dry mass (c, d) of *Vigna radiate* at different treatment period. Significant result denoted by asterists (*, $P < 0.05$)

2.1 *Statistical Analysis*

The data for growth parameters of Mung bean exposed to UV-A (366 nm) and UV-C (254 nm) for 2, 4 and 6 hours were analyzed using "COSTAT" statistical program by two-way analysis of variance (ANOVA) to compare the means of different treatment. "SIGMA PLOT" program was used for graphical representation of data.

3. RESULTS AND DISCUSSION

Germination test of UV irradiated seeds revealed that mean germination rate was increased in UV-A (366 nm) and UV-C (254 nm) irradiated seeds as compare to control (Table 1). Result obtain for final germination percentage was statistically significant ($P< 0.05$). The present investigation showed that UV irradiation causes more rapid germination of seeds. This is probably due to the fact that UV photons (<400nm) are more energetic than visible light photons (>400nm) and, hence

have a stronger effect on the surface of the plant cell [11]. According to an other report stronger effect of UV on plant surface cell causes the ultimate break down of seed coating allowing germination to occur [12].

The effect of UV-A (366 nm) and UV-C (254 nm) radiation on dry mass production and specific leaf area parameters was showed in (Fig. 1). Both total dry mass production and specific leaf area of plant was showed significant ($P< 0.05$) increased, which was more pronounced in UV-A treatment as compare to UV-C treatment. Similar trend was observed for shoot and root length (Fig. 2). Positive effect of UV radiation on growth parameters is substantiation for its regulatory role in photomorphogenesis [13]. Lingakumar & Kulandaivelu have reported that growth has also been promoted by the supplementation of UV in *Cymopsis* seedlings [14]. Enhanced UV radiation promotes vegetative growth possibly via the stimulation of Indole acetic acid (IAA) biosynthesis [13]. Middleton & Teramura have also observed that the combination of visible light and UV, at a particular ratio, is highly suitable for enhanced seedling development[15].

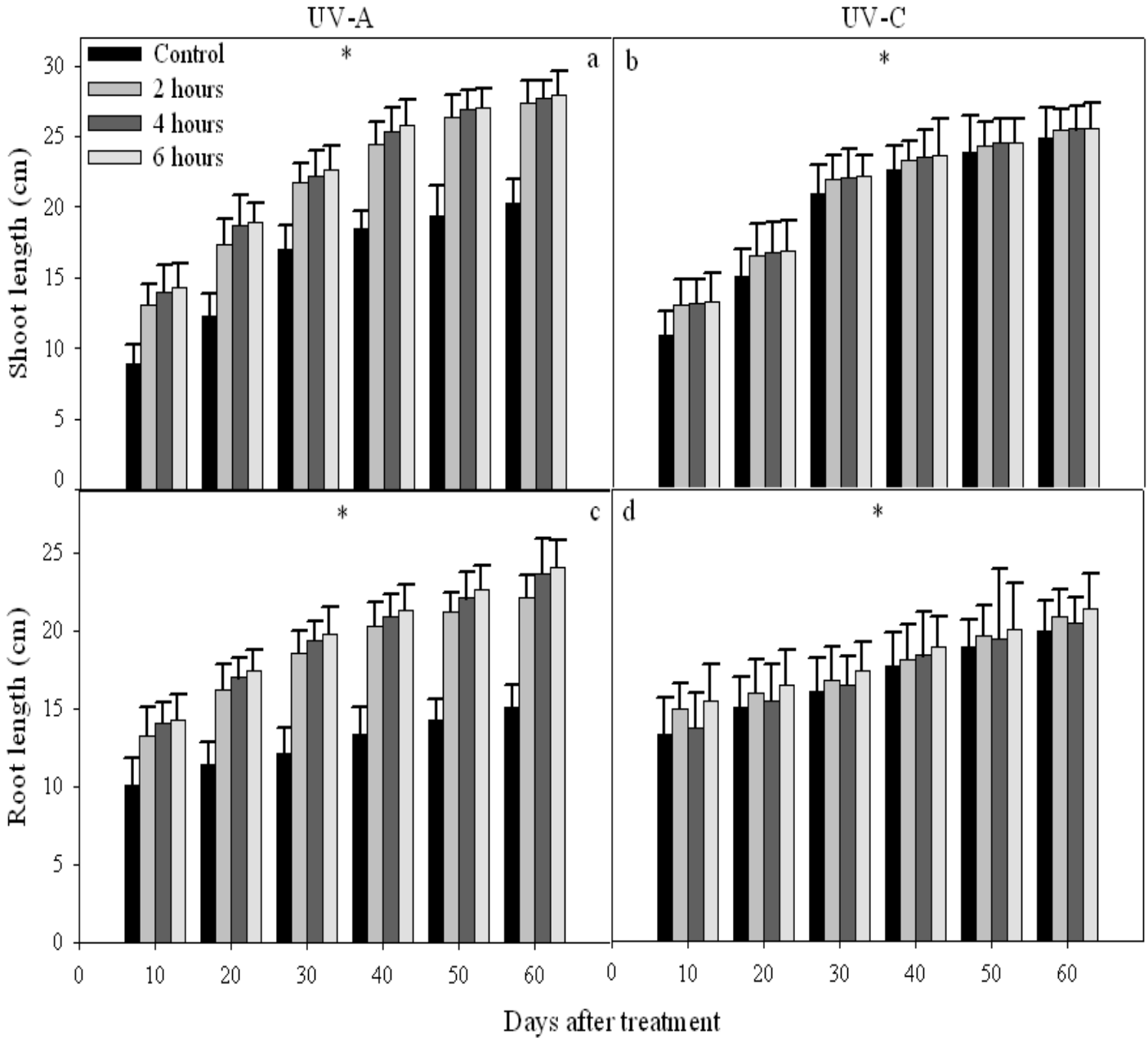

Fig-2: Effect of UV-A and UV-C enhanced radiation on shoot length (a, b) and root length (c, d) of Vigna radiate at different treatment period. Significant result denoted by asterists (*, $P < 0.05$)

4. CONCLUSION

The present investigation showed that pre-treatment of seed with UV-A (366 nm) radiation improves the germination rate, specific leaf area, dry mass, root and shoot length as compare to UV-C (254 nm) exposed seed.

Table-1: Effect of UV-A and UV-C enhanced radiation on germination rate of *Vigna radiata* at different treatment period.

Treatment period (Hours)	UV-A		UV-C	
	No. of germinated seed	Germination rate (%)	No. of germinated seed	Germination rate (%)
Control	16	80	16	80
2	18	90	18	90
4	19	95	17	85
6	20	100	17	85

5. REFERENCE

1. Agrawal, S.B., M. Agrawal, E.H. Lee, G.F. Kramer and P. Pillai. Changes in polyamine and glutathione contents of a green alga *Chlorogonium elongatum* (Dang.) France exposed to mercury. *Envir Exp Bot.,* **(1992)** 32(2): 145-151.
2. Hao, H., B.A. Hale, D.P. Ormrod and A.P. Papadopoulos. Effects of pre-exposure to ultraviolet-B radiation on responses of tomato (Lycopersicon esculentum cv. New Yorker) to ozone in ambient and elevated carbon dioxide. *Envirnomental pollution,* **(2000)** 110: 217-224.
3. Madronich, S. and F.R. de Gruijl. Stratospheric ozone depletion between 1979 and 1992. Implications for biologically active ultraviolet-B radiation and non-melanoma skin cancer incidence. *Photochemistry and Photobiology,* **(1994)** 59: 541–546.
4. Baker, J.T., L.H. Allen and Jr. Assessment of the impact of rising carbon dioxide and other potential climate changes on vegetation. *Environmental Pollution,* **(1994)** 83: 223-235.
5. Strid, A., W.S. Chow and J.M. Anderson. UV-B damage and protection at the molecular level in plants. *Photosynth. Res.,* **(1994)** 39: 475-489.
6. Tevini, M. Effects of enhanced UV-B radiation on terrestrial plants. In: Tevini, M. (Ed.), UV-B Radiation and Ozone Depletion. *Lewis Publishers, Boca Raton, FL,* **(1993)** pp. 125-154.
7. Mpoloka, S.W. Effects of prolonged UV-B exposure in plants. *African Journal of Biotechnology,* **(2008)** 7(25): 4874-4883.
8. Jansen, M.A.K., V. Gaba and B.M. Greenberg. Higher plants and UV-B radiation: balancing damage, repair and acclimation. *Trends in Plant Science,* **(1998)** 3: 131-135.
9. Fukushima, A. and K. Saito. Influence of UV-light on carthamin accumulation and floret elongation in a cultivar of saffron thistle (*Carthamus tinctorius* L.). *Acta Physiologiae Plantarum,* **(2000)** 22(2): 159-162.
10. Choi, B.Y. and K.S. Roh. UV-B radiation affects chlorophyll and activation of Rubisco by Rubisco activase in *Canavalia ensiformis* L. leaves. *J Plant Bio.,* **(2003)** 146: 117-121.
11. Kovacs, E., A. keresztes. Effect of Gamma and UV-B/C radiation on plant cells. *Micron.,* **(2002)** 33(2): 199-210.
12. Noble, R.E. Effects of UV irradiation on seed germination. *The Science of the Total Envirnoment,* **(2002)** 299: 173-176.
13. Jayakumar, M., P. Amudha and G. Kulandaivelu. changes in growth and yield of *Phaseolus mungo* L. induced by UV-A and UV_B enhanced radiation. *Journal of Plant Biology,* **(2003)** 46(1): 59-61.
14. Lingakumar, K. and G. Kulandaivelu. Differential responses of growth and photosynthesis in *Cymopsis tetragonoloba* L. grown under ultraviolet-B and supplemented longwavelength radiation. *Photosynthetica,* **(1998)** 35:335-343.
15. Middleton, E.M. and A.H. Teramura. Understanding photosynthesis, pigment and growth responses induced by UV-B and UV-A irradiances. *Photochem Photobiol.,* **(1994)** 60: 38-45.

Pak. J. Chem. 1(4):168-175, 2011 Full Paper
ISSN (Print): 2220-2625
ISSN (Online): 2222-307X

Instruction Manual of Systemic Approach to Teaching and Learning (SATL)

[*]M. Nazir and I. I. Naqvi
[*]Department of Chemistry, University of Karachi, Karachi-75270, Pakistan
National Core Group in Chemistry, H.E.J Research Institute of Chemistry, University of Karachi, Pakistan
Email: [*]nazir_misbah@yahoo.com

ABSTRACT
In order to have better understanding of scheming of lectures via Systemic Approach to Teaching and Learning (SATL) method examples of daily life have been selected. In this practice different thoughts are arranged in a way that the correlations between a variety of concepts becomes explicable.

Keywords: Systemic approach, teaching method, effective learning, lecture designing.

1. INTRODUCTION
Linear approach of teaching, which is in vogue throughout the world at the moment, is based upon step by step transfer of information to students, who are subsequently expected to link the various segments of knowledge on their own. This approach encourages rote learning, hinders creativity and is thus not advisable any more. On the other hand, recently introduced Systemic Approach to Teaching and Learning (SATL) methodology is a holistic in essence and encompasses delivery of facts, concepts and skills in one package. Consequently, a web of knowledge is constructed. Teaching community across the globe is gradually responding to this recently introduced technique. This mode of teaching is increasingly getting appreciation and generating enthusiasm among the world academia. Being a new mode of teaching, sufficient books and lessons, are not freely available for this methodology.
Nevertheless, those who get involved in the mental exercise of promoting this mode of learning, start enjoying it.
Teaching is carried out through communication. Learning process becomes pleasant if better communication skills of teacher; prevail upon the inherent inertia, associated with the students, while they focus upon a difficult subject. SATLC technique is a better instrument for making the teacher's job easier, as it amply enhances the communication skills of the teacher.

2. METHODOLOGY
Any teacher who wishes to join this caravan of knowledge will be able to facilitate by building teaching units and undertake unified effort involving numerous steps detailed below:

1. **Enlist your aims and the operational objectives of concerning lesson such that systemic aims are clearly addressed**

For example aim of the lesson is to introduce a person.

2. **Identify the perquisite for teaching the desired lesson from previous study**

Further to that salient features of the lesson that incorporate facts, concepts, laws, interrelationships and subsequent skills, to be accrued from the teaching and learning exercise, are to be underlined and elaborated
Students will be able to recognize the person, from different aspects of his personality. We need addressing the following issues.

- Achievements
- Qualification
- Field of interest
- Personality
- Nature of job
- Responsibilities etc.

3. **Develop a diagram which demonstrates linear connections between the concepts already outlined above**

The diagram that develops for projecting the person, on the basis of these undertakings is reproduced below

*Corresponding Author Received 15th August 2011, Accepted 10th September 2011

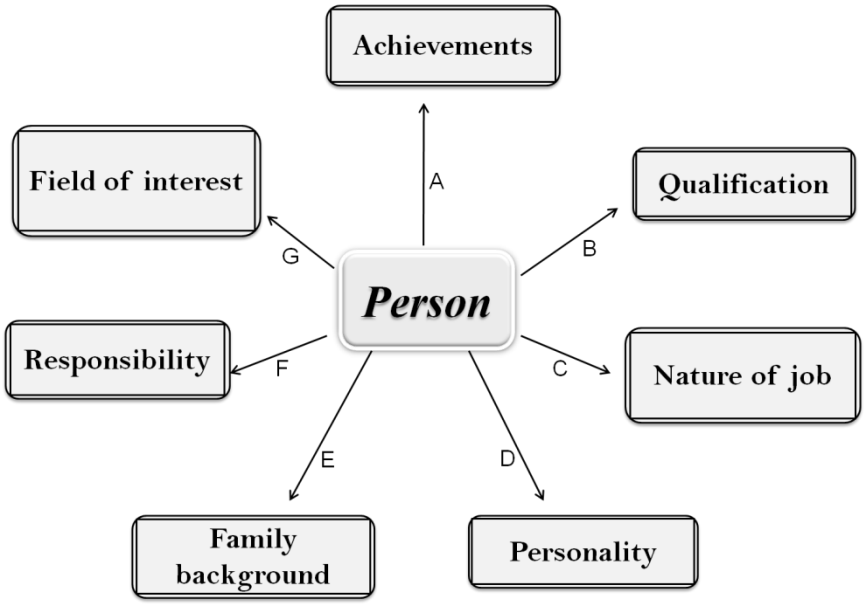

Fig-1: Illustration of linear connections between important concepts

This diagram describes the basic concepts pertaining to the lesson with its relevant information. Here, it is to be noticed that the above connections are linear and independent from each other.

4. **Mark the already known connections, from previous knowledge, with tick sign (√). Then identify the remaining connections which are unknown by putting question mark sign (?) on the connectivity line**

The modified diagram is shown in Fig-2.

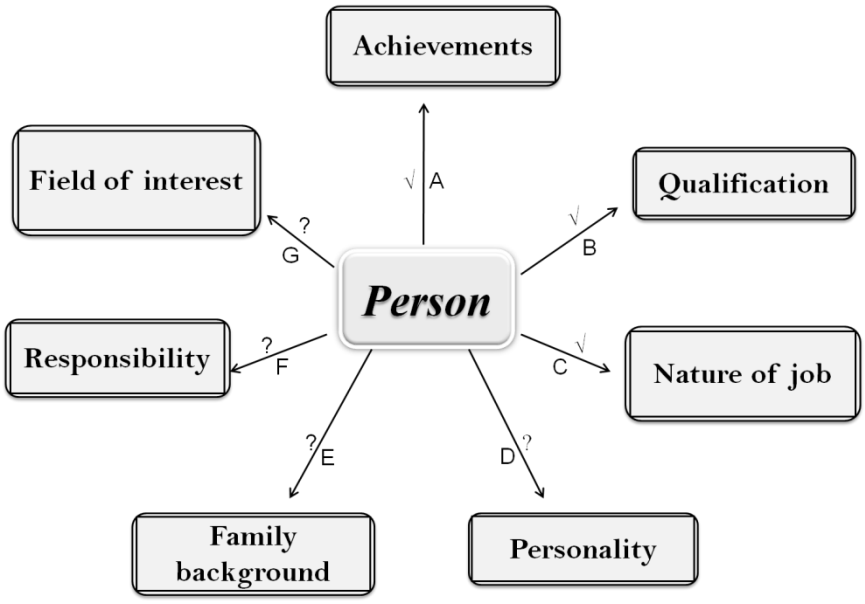

Fig-2: Linear connections between important concepts having tick mark signs (√) on the known connections and question mark signs (?) on the unknown connections

5. **The diagram developed on the basis of suggestions in the previous step, out lines the linear relationships in an orderly manner. It is to be modified to a systemic diagram. This can be done by placing the respective relations between the concepts as shown in the diagram**

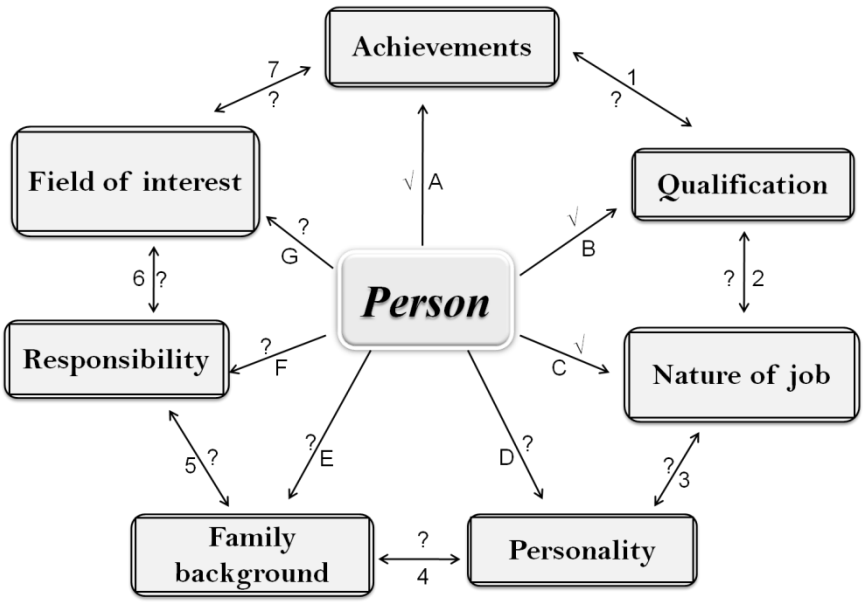

Fig-3: Systemic Diagram (SD-0)

This is going to be the first diagram of its kind in a series of diagrams that is expected to be illustrated during teaching and learning exercises. Let us call it to be diagram SD-0.
From the systemic diagram SD-0 one can notice the following.

a) Known relationships are well illustrated in this diagram through the tick sign (√).
b) The unknown relationships of diagram SD-0 bear the question mark sign (?).

6. **Now we come to another stage of lesson development where some of the undefined relationships of SD-0 are defined by the teacher and students are asked to replace few of the (?) marks on the diagram SD-0 by (√) marks. This will be done to those unknown relationships of SD-0, which are just learned from the teacher. Thus we arrive at diagram SD-1**

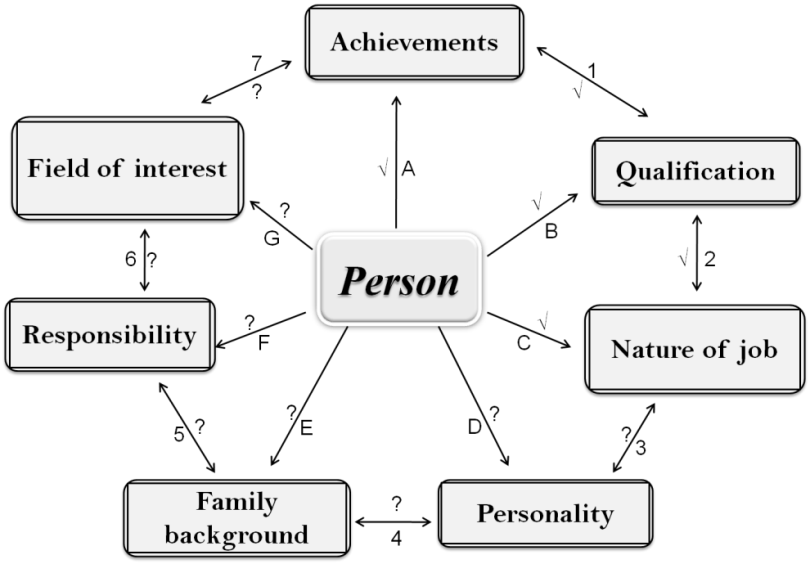

Fig-4: Systemic Diagram (SD-1)

We must note now that diagram SD-1 is composed of two types of interrelationships, one which are known, as they are clearly taught by the teacher and students have put on (√) mark on the account of their understanding. The second component with sign (?) are still unknown and hence to be debated in the class. The ensuing discussion, guides us to unfold secrets behind some more unknown. Following this class discussion and resulting conclusions, some of the (?)

marks are also replaced by (√) marks on the diagram to symbolize them as known. This debate in the class about unknown concepts in relation to known ones will result in building new systemic relationships and also help the teacher to assess the systemic understanding of the proceedings part by part.

When the debate proceeds further one can go deeper and deeper into the conceptual interface of the subject and identify newer relationships and when these are brought the diagram SD-1, it is converted into SD-2.

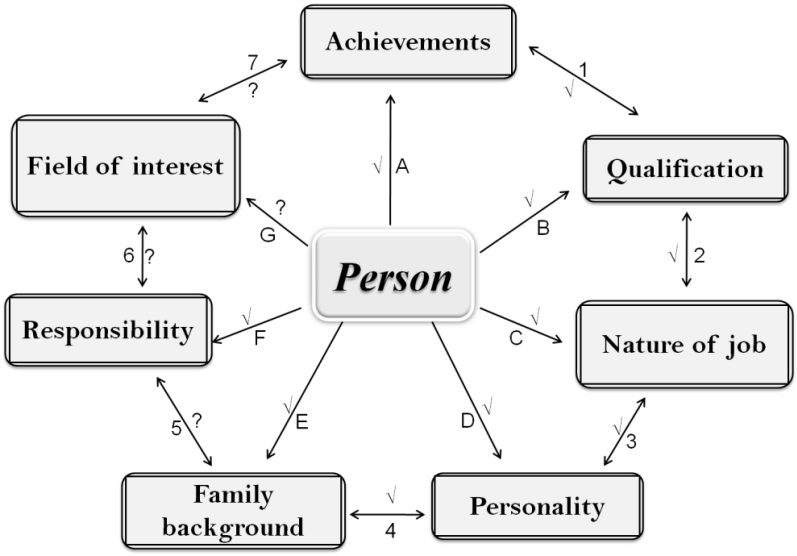

Fig-5: Systemic Diagram (SD-2)

A glance at SD-2, helps to appreciate and notice the following:

a) All the relationships have been identified except few, which have to be developed in the later stage of the lesson.
b) At this stage of study, the students are required to ponder upon the relationships developed during the debate and try to develop the remaining unknown relationships.
c) It is expected that at this stage of learning students could build several systemics of their own.

7. At this stage we come closer to our goal and even the remaining unknown relationships of SD-2 are known now and these are placed on SD-2 to obtain SD-3 diagram. The diagram SD-3 has answers pertaining to all unknown relationships and thus the learning unit gets completed

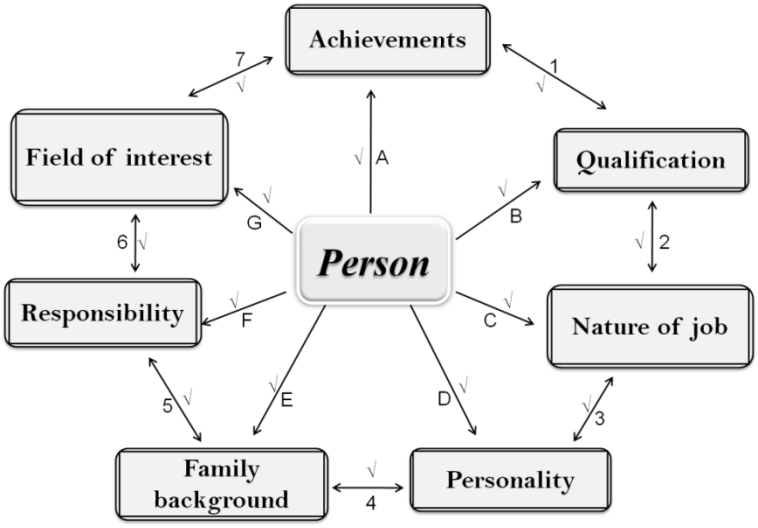

Fig-6: Systemic Diagram (SD-3) or (SDf)

This diagram SD-3 may be called the terminal systemic diagram or final systemic diagram (SDf).
Let us summarize what we have achieved in the above course of discussion.

- SATL units involve development of stage wise systemic diagrams (SD-0, SD-1, SD-2 and SD-3). These diagrams have SD-0 as a starting point and SD-3 as terminal point of the course in between them are SD-1 and SD-2 stages.
- The SATL teaching lessons are marked as SD-0, SD-1, SD-2 and the last SD-3. All of them are essentially similar except they differ in the counts of tick signs (√), the known relationships, and the counts of question marks (?), which represent the unknown ones. As the course progresses the (√) signs grow on the cost of (?). This scenario is diagrammatically described through following figure.

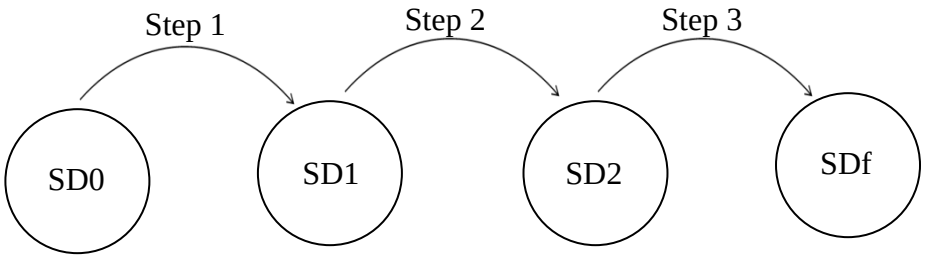

Fig-7: Systemic approach stratagem

- This is quite evident now that systemic approach develops comprehension against usually practiced technique of preparing notes for memorization. It enables the teacher to continue refining his/her teaching skills and the students ensure to accumulate knowledge through learning as the course proceeds.

- The students are allowed to tread upon a pathway of knowledge, as the teaching units unfold newer horizons of information. This motivates the students for developing interconnectivities with information imparted to them at various stages of SATL discourse and their basic inputs of the past. These exercises will make the students capable of finding new avenues of knowledge and build a correct cognitive structure.

- At the culmination of the lesson, the students may be advised to develop newer systemics of their own. This gives the teacher a chance to evaluate the student comprehension of the unit lesson through final systemic assessment.

Let us ponder another example for treating SATL path. We want to enlighten a group of knowledge seekers about a city. This SATL lesson would require the following multi step progress.

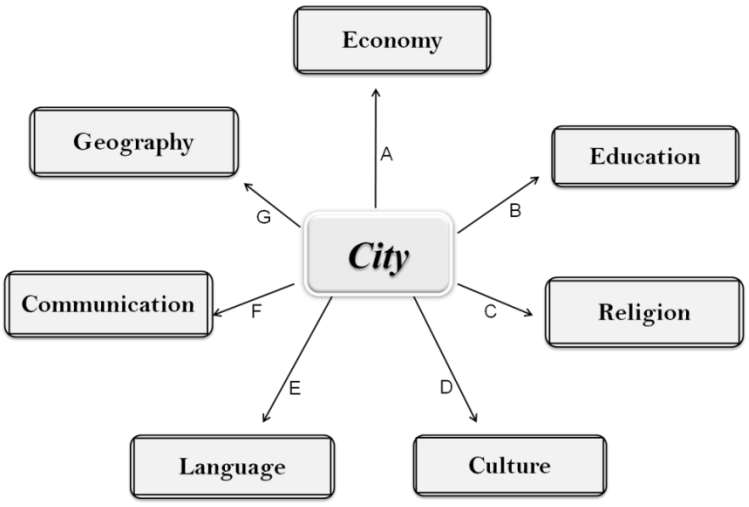

Fig-8: Illustration of linear connections between important concepts

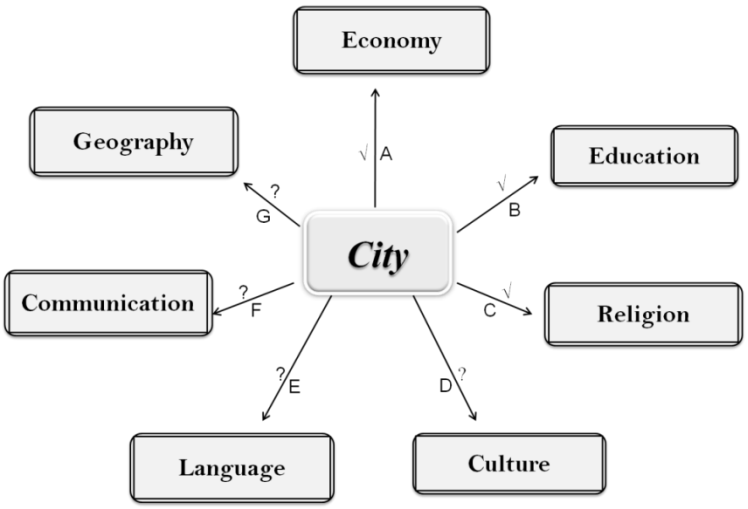

Fig-9: Linear connections between important concepts having tick mark signs (√) on the known connections and question mark signs (?) on the unknown connections

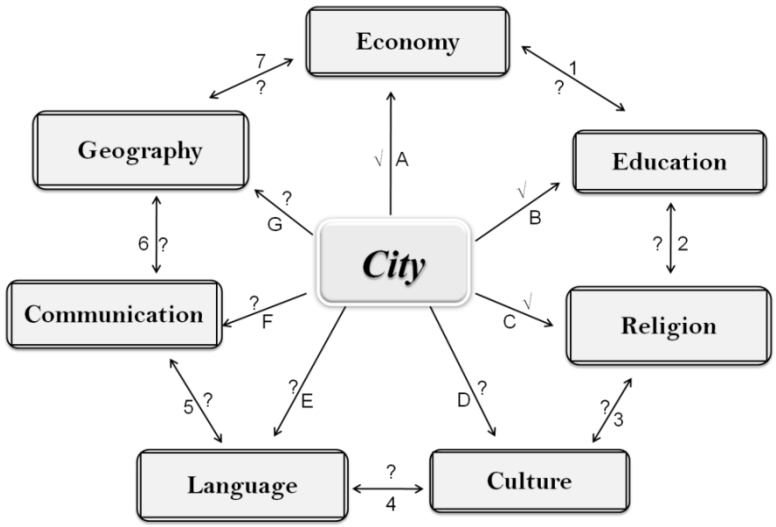

Fig-10: Systemic Diagram (SD-0)

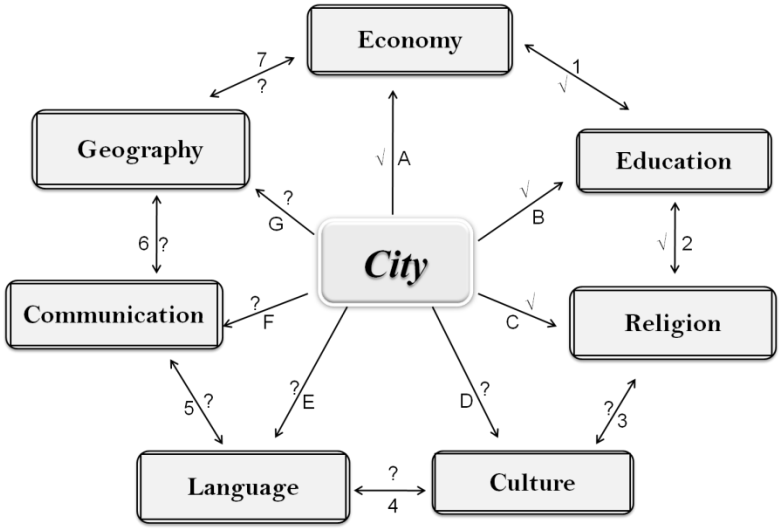

Fig-11: Systemic Diagram (SD-1)

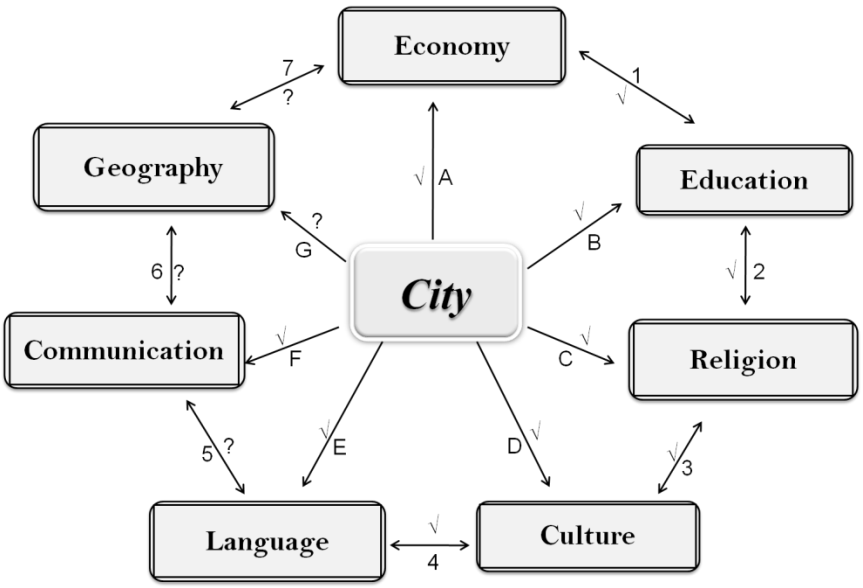

Fig-12: Systemic Diagram (SD-2)

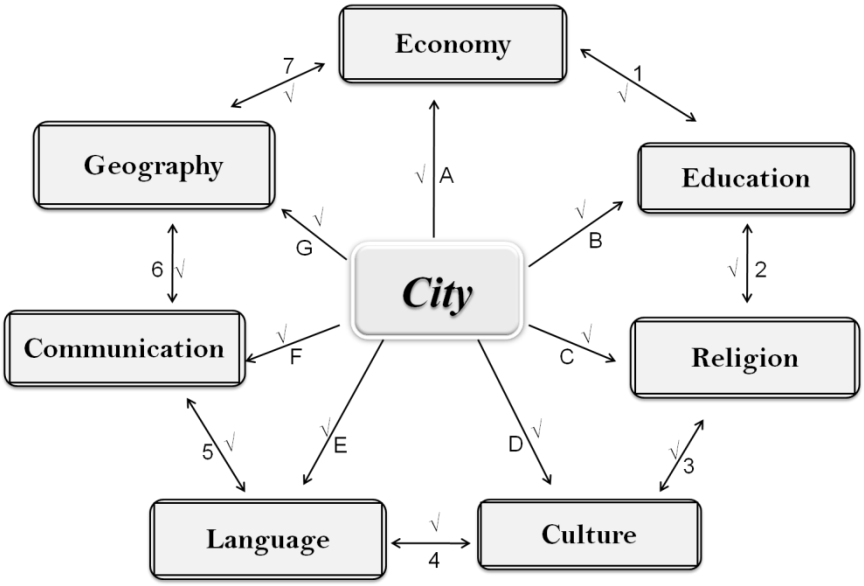

Fig-13: Systemic Diagram (SD-3) or (SDf)

While going into further details of the topic, the teacher may even develop several systemic diagrams on a variety of topics.

3. SUMMARY

Designing of lecture by using Systemic Approach to Teaching and Learning methodology has been demonstrated though common examples. However, this method can be utilized to enlighten topics of a particular subject like Chemistry[1-7]

4. REFERENCES

1. Fahmy A. F M. and Lagowski J. J Chemical Education International **(2001)** 3 (1).
2. Fahmy, A. F. M., Lagowski, J. J. Systemic Reform in Chemical Education an International Perspective, J. Chem. Edu. **(2003)** 80 (9), 1078.
3. Fahmy, A. F. M., Lagowski, J. J. The systemic approach to teaching and learning (SATL): A 10-year review, AJCE, **(2011)** 1(1) 29-47.

4. Fahmy, A. F. M., Lagowski, J. J. The systemic approach to teaching and learning (SATL): Operational steps for building teaching units, AJCE, **(2011)** 1(1)62-80.
5. Fahmy, A. F. M., Said, A. The systemic approach to teaching and learning: Water chemistry, AJCE, **(2011)** 1(2)50-58.
6. Nazir, M. and I. I. Naqvi, I.I. Systemic approach to teaching and learning chemistry (SATLC) as integrated approach towards teaching physical chemistry, **(2011)** AJCE, 1(2)59-71.

Pak. J. Chem. 1(4):176-184, 2011 Full Paper
ISSN (Print): 2220-2625
ISSN (Online): 2222-307X

Redox process in [*N*-(2-hydroxyethyl)-ethylene-diamine-*N*,*N*′,*N*′-triacetato] uranium (IV)

[*]R. Perveen , M. Ashfaq and I. I. Naqvi[1]
[*]Department of Chemistry, University of Karachi-75270
[1]NCGC, HEJ Research Institute of Chemistry, ICCBS, University of Karachi Pakistan
E-mail: [*]rasa_19782000@yahoo.com

ABSTRACT

The kinetics of reduction of tris(1, 10 orthophenanthroline) iron(III) by [*N*-(2-hydroxyethyl)-ethylene-diamine-*N*,*N*′,*N*′-triacetato] uranium (IV), symbolized as [U(IV) HEDTA]$^{1+}$, has been investigated in aqueous medium at 30 ± 0.5 ^{o}C . Measurements were recorded under pseudo first order conditions. The rate of electron transfer reaction between these reactants was measured by varying pH and ionic strength, between 2.5-3.0 and 0.01-0.05 M respectively. It was found that pH directly influenced the k_1 and values were found to be 111.8, 193.7, 344.7 478.93 mol^{-1} dm^{3}s^{-1} at pH 3.2, 3.0, 2.8, 2.5 respectively. The value of k' was evaluated as 6.35× 10^6 mol^{-1} dm^{3}s^{-1}.

Abbreviations: EDTA = Ethylene-diamine-*N*,*N*′,*N*′-tetra acetic acid, HEDTA = [*N*-(2-hydroxyethyl)-]ethylene-diamine-*N*,*N*′,*N*′-triacetatic acid

Keywords: kinetics, ionic strength, pH and HEDTA.

1. INTRODUCTION

Uranium, a f block element, is found in Earth's crust at an average concentration of about 2 ppm, and is more abundant than silver or mercury. The most common uranium-containing mineral is uratinite, a complex uranium oxide. Ionic liquids replace organic liquids used in different processing operations related to f block elements[1]. For example, hydrophobic ionic liquids are used in liquid/liquid f-element extraction processes, based upon electrode deposition. For f-element-catalyzed reactions, high reaction rates, enhanced selectivity, better immobilization of the catalyst and an easy product recovery has often been observed in certain ionic liquids.[1] The electro-deposition of uranium oxide (possibly UO_2) from UO_2^{2+} and its behavior in much ionic liquid has been studied in ionic liquid. At high temperatures, the cathodic peak potential shifts for the reduction of U(VI) to UIV towards more negative triethyloctylammonium),[N222(12)][Tf2N] (triethyldodecylammonium)[3,4]. A review of the thermodynamic data for the different oxidation states of actinide compounds with citrate, isosaccharinate and polyaminocarboxylate complexes has underlined their importance for environmental modeling.[5] The computational Chemistry give an insight into electronic structure of f- elements.[6] The synthesis and reactivity behavior of uranium (IV) complexes has been described by many scientists.[7-14]
The substitution and redox behavior of polyamino carboxylate complexes of metal ion complexes have found increased interest from researchers in last few years.[14-21]

HEDTA becomes an important ligand and many studies have been made on different complexes of HEDTA and between different metals in presence of HEDTA. The interaction of [Ru(III)(HEDTA) H_2O)] with a series of selected thiols having extra functional groups was investigated potentiometrically and kinetically. The effect of dioxane on the pK(a) values [Ru(III)HEDTA (H_2O)] and the formation constants of the corresponding thiol complexes was also presented.[14] Fe(II)L; L = EDTA, HEDTA, tcma (tcma = 1-acetato-1,4,7-triazacyclononane) with hydrogen peroxide in neutral and slightly acidic solutions was studied by using the beta elimination reaction as an assay for the formation of hydroxyl free radicals, OH.[15] The complexation of Fe(II) with HEDTA results in the decrease of redox potential, and enhances the reducting ability of Fe(II). An important example is the use of Fe(II)-organic complexes to accelerate Cr(VI) reduction.[19] The study has been made to evaluates the inhibition of Cr(III) oxidation by Mn oxide in the presence of HEDTA.[20] The kinetics of the oxidation of [*N*-(2-hydroxyethyl)-ethylene-diamine-*N*,*N*′,*N*′-triacetato] cobalt(II), ([Co^{II}-(HEDTA)]$^{1-}$, by *N*-bromosuccinimide (NBS), has been studied in aqueous solutions and water-methanol solvent mixtures under various conditions . An inner sphere mechanism is proposed for p oxidation of both the protonated and deprotonated species of the complex, with the formation of an intermediate which slowly forms the final oxidation product, [Co^{III}(HEDTA)]$^{1-}$. In water-methanol solvent mixtures the reaction rate decreased as the methanol content was increased.[21] Similarly periodate ion oxidation of varieties of [CoIIL(H2O)]2-n complexes (L = EDTA, HEDTA, NTA, DTPA, PDTA, and HPDTA) have been investigated following the inner sphere mechanism.[22] A comparative study of the kinetics of the reaction of superoxide radical with Fe(II1)complexes of EDTA, DETAPAC and HEDTA was also ade.[23] Uranium complex of N-hydroxyethyl-ethylenediamine-triacetic acid (HEDTA) has been prepared by Martel et al.[24]

*Corresponding Author Received 7th November 2011, Accepted 16th November 2011

Oxidation of different complexes of Uranium (IV) polyamino carbooxylates with Tris 1, 10 orthophenanthroline iron (III) has been studied and reported by us previously.[5-27] Redox process in Uranous [N- (2- hydroxyethyl) - ethylenediamine triacetate has been studied in the current investigations.

2. EXPERIMENTAL

Tris 1, 10 orthophenanthroline iron (III) – perchlorate was prepared by the method described by N. Sutin and B.M.Gordon[27] 0.1M stock solution of uranyl nitrate was prepared by dissolving an appropriate amount of uranyl nitrate (Aldrich Anal R grade) in 0.1 M HCl. Uranous solution was obtained by catalytic hydrogenation of uranyl nitrate.[28] Uranous solution has been standardized against potassium dichromate solution.[29] 0.1 1M stock solution of HEDTA was prepared by trisodium salt of N- (2-hydroxyethyl)- ethylenediamine triacetate dihydrate (HEDTA). Standard U(IV) solution , warmed up to 40 – 50 $^{\circ}$C, was mixed with HEDTA solution to get [U(IV) HEDTA $2H_2O$]Cl . No precipitate appeared, as the dark leaf green solution of $[U(IV)\ HEDTA]^{1+}$ has high solubility in water .The pH of $[U\ (IV)\ HEDTA]^{1+}$ solution was maintained up to 3.0.

2.1 *Spectrophotometric Determination of [U(IV)HEDTA]Cl*

In order to determine the stability constant of $[U(IV)HEDTA]^{1+}$ at μ = 0.1M (NaCl) and 25 ^{o}C , a competition reaction between Th(IV), U(IV) and HEDTA was employed. The experiment was carried out at pH = 1.4-1.5. At these pH values the rate of polymerization of UOH^{3+} is slow[28] and it was also assumed that no hydroxo or polynuclear specie of [U(IV) HEDTA]$^{1+}$ are likely to be present in solution. The absorbance of a 1:1:5 U(IV) –HEDTA-Th(IV) solution was obtained at λ = 659 nm. Of the various species present in the competition reaction, U(IV) , UOH^{3+}, and $[U(IV)HEDTA]^{1+}$, Th(IV)HEDTA and Th(IV) , only the UOH^{3+} , $[U(IV)HEDTA]^{1+}$ and U(IV) absorb in the region of interest. The spectra of U(IV) UOH^{3+} had been investigated previously by Kraus and Nelson.[30] There is a shift of peak of U(IV) to longer wave length 659 nm after complexation. Differences in extinction coefficient at 659 and 700 nm were used for calculation rather than absolute value of extinction coefficient at one wavelength. By using the hydrolysis constant for U(IV) at 0.1M ionic strength previously determined by Kraus and Nelson[29] and molar extinction coefficient for three U(IV) species, it is possible to measure the concentration of each of the three U(IV) specie in solution, using the usual relationship.

$$A = \varepsilon_{U\text{-}HEDTA}(1)[UOH^{3+}\ \varepsilon_{U}(1)[U(IV)] + \varepsilon_{U\text{-}OH}\,(\,1)[U\text{-}HEDTA]^{1+}$$

Where $\varepsilon_{U\text{-}HEDTA}$= 52, ε_{U} = 22 and $\varepsilon_{U\text{-}OH} \approx 3.0$ Thus by measuring the absorbance of a 1:1:5 U(IV)-HEDTA-Th(IV) solution and knowing the stability constant of Th(IV)HEDTA previously determined it was simpler mater to determine the equilibrium constant .

$$Th(IV)\text{-}HEDTA + U(IV) \leftrightarrow [U(IV)HEDTA]^{1+} + Th(IV)$$

The value for $K_{U\text{-}HEDTA}$ is thus obtained. The same result was obtained for equilibrium constant by changing the order of addition of the various reagents indicating that equilibrium is reached rapidly. The value of logarithm of stability constant was found to be 21.

3. RESULT AND DISCUSSION

3.1 *Determination of Order of Reaction with Respect to [Fe (opt)$_3$]$^{3+}$*

Results of the kinetic measurements for the reduction of [Fe (opt)$_3$]$^{3+}$ by [U(IV) HEDTA]$^{1+}$ are being reported in the Tables 1 and 2**.** Pseudo first order condition was applied to observe the effects. The concentration of [U(IV) HEDTA]$^{+}$ was maintained at ten times excess over the corresponding [Fe (opt)$_3$]$^{3+}$ concentration. Psuedo first order rate constant (k_{ob}) was obtained by plotting ln (A_α - A_t) vs. time (Figure 4) , for varying concentrations of [Fe (opt)$_3$]$^{3+}$ whereas other parameter have been held constant. As shown in Table 2 these values of the rate constant turn out to be reasonably constant while the concentration of [Fe (opt)$_3$]$^{3+}$ is increased .

3.2 *Indirect Determination of Order of Reaction with Respect to [U (IV) HEDTA]$^{1+}$*

By varying [U (IV) HEDTA]$^{1+}$ concentrations the corresponding values of pseudo first order rate constant (k_{obs}) were calculated to evaluate the order of reaction with respect to [U(IV) HEDTA]$^{+}$ at different pH conditions (Tables 3-7). The other parameters are kept constant. The plot of k_{obs} values against [U(IV) HEDTA]$^{1+}$ concentration gives a straight line passing through the origin Figure 6. Pseudo first order rate constant is linearly related to the concentration of [U(IV) HEDTA]$^{1+}$ and thus the order of reaction with respect to [U(IV)HEDTA]$^{1+}$ is also first. The second order rate constant (k_1) at different pH conditions has been found to be k_1 =111.85, 193.68, 344.7 and 640.19 $M^{-1}s^{-1}$ at pH 3.2, 3.0, 2.8 and 2.5.

3.3 *Dependence of the Hydrogen Ion Concentration*

Hydrogen ion concentration affected the concentration of protonated specie and enhanced the reaction rate as shown in Table 8 and 9 at constant temperature of (30 °C). The following equation gives the order of the reaction with respect to hydrogen ion concentration [H^+]

$$\text{Rate} = Kk'[H^+]^n\ [U(IV)\ HEDTA]^{1+}\ [Fe\ (opt)_3]^{3+} \quad \textbf{(1)}\ \text{At constant pH}$$

$$k_{obs} = k_1[U(IV)HEDTA]^{1+} \quad \textbf{(2)}$$

$$k_1 = Kk'[H^+]^n \quad \textbf{(3)}$$

K is the equilibrium constant for the protonation of $[U(IV)\ HEDTA]^{1+}$ and k' is the specific rate constant for the reaction between $[\ U(IV)\ HEDTA(H^+)]^{1+}$ and $[\ Fe\ (opt)_3]^{3+}$. $Kk'[H]^n$ is the k_1 for each experiment at constant pH. k' equals to $.35 \times 10^6$ $dm^3mol^{-1}s^{-1}$ .evaluated from the slope of the plot of k_1 vs H^+ concentration (Figure 7). From the slope of a plot of log [H^+] against log k_{obs} , at constant temperature, the value of n can therefore be concluded and it equals to 1.2 This is nearly equal to value of n being 1. The corresponding plot is shown in Figure 7-8. It is therefore suggested that the rate of oxidation of $[U(IV)\ HEDTA]^{1+}$ by $[Fe\ (opt)_3]^{3+}$ is dependent on the first power of hydrogen ion concentration.

3.4 *Effect of Ionic Strength on the Reaction Rate*

Rate of reaction got increased with the increase in ionic strength, which was varied between 0.01 to 0.05M Table-10. This increase in the k_{obs} may be a result of the charges on $[Fe\ (opt)_3]^{+3}$ and $[\ U(IV)\ HEDTA]^{1+}$ the main reacting species. By plotting a graph between $\mu^{1/2}$ and k_{obs} product of charges, $Z_A\ Z_B$ for the reactants, was evaluated and it equals to +3.02 (Figure 9). This ionic strength effect also confirmed that the reaction follows the outer sphere kinetics. Although the HEDTA complex has OH group for the bridge but no evidences for the bridging was found. The situation is similar to the reaction between $Co(EDTA)^{1-}$ and $Fe(CN)_6^{3-}$, where a possibility of inner sphere mechanism has been ruled out even in the presence of a of bridging CN group and outer sphere mechanism has been advocated[31-32] Since $[Fe\ (opt)_3]^{3+}$ of the two complexes is inert for substitution so the outer sphere mechanism is strongly supported for the electron transfer between $[U(IV)\ HEDTA]^{1+}$ and $[Fe\ (opt)_3]^{3+}$

3.5 *Effect of Temperature on the Reaction*

Effect of temperature on the rate of a reaction is used for the determination of thermodynamic parameters. As shown in the Table 11, the rate of reaction was found to increase from 114 to 288 $M^{-1}\ s^{-1}$ while the temperature is increased from 10 ^{0}C to 35 ^{0}C. A plot of $\ln k_1$ against 1/T is linear (Figure 10). Thermodynamic parameters are listed in Table-12.

3.6 *Proposed Mechanism*

$$[U(IV)HEDTA]^{1+} + H^+ \xleftrightarrow{K} [U(VI)HEDTA(H^+)]^{1+1} \quad \textbf{(4)}$$

$$[U(IV)HEDTA(H^+)]^{1+} + [Fe(opt)_3]^{3+} \xrightarrow{k'} [U(V)HEDTA(H^+)]^{2+}[Fe(opt)_3]^{2+} \quad \textbf{(5)}$$

$$[U(V)HEDTA(H^+)]^{2+} + [Fe(opt)_3]^{3+} \xrightarrow{k_2} [U(VI)HEDTA(H^+)]^{3+}[Fe(opt)_3]^{2+} \quad \textbf{(6)}$$

Net reaction

$$[U(IV)HEDTA]^{+1} + [Fe(opt)_3]^{3+} \longrightarrow [U(VI)HEDTA]^{3+}[Fe(opt)_3]^{2+}$$

$$\text{Rate} = \frac{d[Fe(opt)_3]^{2+}}{dt} = k_1\ [U(IV)\ HEDTA]^{+1}\ [Fe\ (opt)_3]^{3+} \quad \textbf{(7)}$$

$$\frac{d[Fe(opt)_3]^{2+}}{dt} = k_{obs}[Fe(opt)_3]^{3+} \quad \textbf{(8)}$$

Hydrogen ion dependence is reflected in the following relationship

$$\text{Rate} = \frac{d[Fe(opt)_3]^{2+}}{dt} = Kk'[H^+]^n\ [U(IV)\ HEDTA]^{1+}\ [Fe\ (opt)_3]^{3+} \quad \textbf{(9)}$$

Expected mechanism describes that k' is specific rate constant for second order rate equation for the reaction between $[U(IV)\ HEDTA(H^+)]^{1+}$ and $[Fe\ (opt)_3]^{3+}$. K is designated as equilibrium constant for the protonation reaction $[U(IV)\ HEDTA]^{1+}$ + [H^+] = $[\ U(IV)\ HEDTA(H^+)]^{1+}$. The second step which involves the reacting specie [U(IV)

$HEDTA(H^+)]^{1+}$nd $[Fe(opt)_3]^{3+}$ will be the slowest out of the three proposed pathways, and that the steps 1 and 3 are assumed to be faster ones. Our observations are likely to support the following assumptions:

1. Mechanism involves an outer sphere pathway.
2. The over all reaction follows second order kinetics.
3. There is an equilibrium between the protonated and deprotonated forms of the $[U(IV)HEDTA]^{1+}$ complex. Effect of ionic strength and pH on the k_{obs} (Tables & 9) showed that the activated complex has +3 charge.
4. The equilibrium shifts towards the protonated specie with the decrease of pH (Table 5).
5. Protonation of the co-ordinated complex facilitates the unwrapping of ligand with the decrease in pH. Thus free U(IV) is made available for the redox reaction[25-27] . So an increase in k_{obs} is observed with the decrease of pH.

Table-1: Effect of $[Fe(opt)_3]^{3+}$ on psuedo first order rate constant (k_{obs})

Serial No.	$10^5 [Fe(opt)_3]^{3+}$/ mol/dm^3	$10^2 k_{obs}/s^{-1}$
1	3.0	11.20 ± 0.22
2	3.5	11.32 ± 0.21
3	4.0	11.19 ± 0.20
4	4.5	11.4 ± 0.23
5	5.0	11.31 ± 0.20

$[U(IV)HEDTA]^{1+} = 6\times 10^{-4}$ mol/dm^3, pH =3.0
Temperature = 30 °C, μ = 0.01 mol/dm^3

Table-2: Effect of $[U(IV)HEDTA]^{1+}$ concentration on psuedo first order rate constant (k_{obs})

S. No	$[U(IV)HEDTA]^{1+}$ 10^4 / mol/dm^3	10^2 k_{obs} / s^{-1}
	pH 2.5	
1	6.0	32.15 ± 0.31
2	7.0	42.34 ± 0.24
3	8.0	52.21 ± 0.25
4	9.0	59.56 ± 0.34
5	10	65.62 ± 0.42
	pH 2.8	
1	6.0	19.32 ± 0.25
2	7.0	23.42 ± 0.25
3	8.0	27.25 ± 0.35
4	9.0	31.87 ± 0.33
5	10	35.34 ± 0.35
	pH 3.0	
1	6.0	11.22 ± 0.23
2	7.0	13.42 ± 0.25
3	8.0	15.25 ± 0.24
4	9.0	17.87 ± 0.25
5	10	19.30 ± 0.24
	pH 3.2	
1	6.0	6.82 ± 0.23
2	7.0	7.52 ± 0.32
3	8.0	8.85 ± 0.35
4	9.0	9.87 ± 033
5	10	11.23 ± 0.32
	pH 3.5	
1	6.0	1.26 ± 0.23
2	7.0	4.31 ± 0.32
3	8.0	5.92 ± 0.25
4	9.0	6.84 ± 0.23
5	10	7.52 ± 0.24

$[Fe(opt)_3]^{3+} = 3.0 \times 10^{-5}$ mol/dm^3, Temperature = 30 °C, μ = 0.01 mol/dm^3

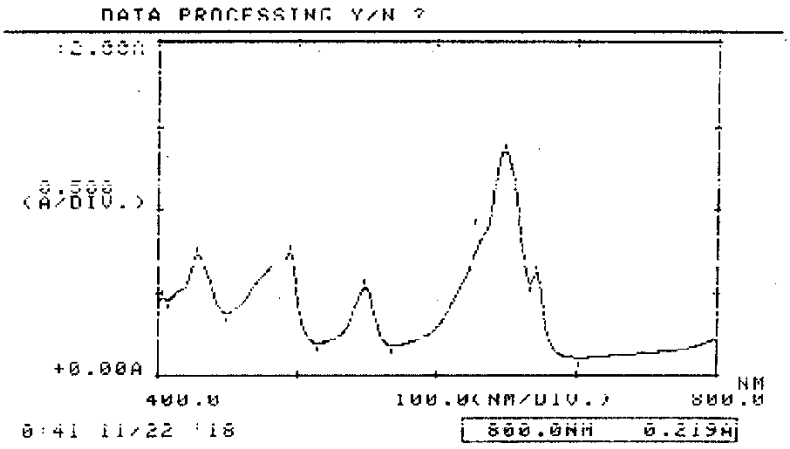

Fig-1: Spectra of 0.03 M $[U(IV)HEDTA]^{1+}$ at pH 3.0 and 0.1 M ionic strength.

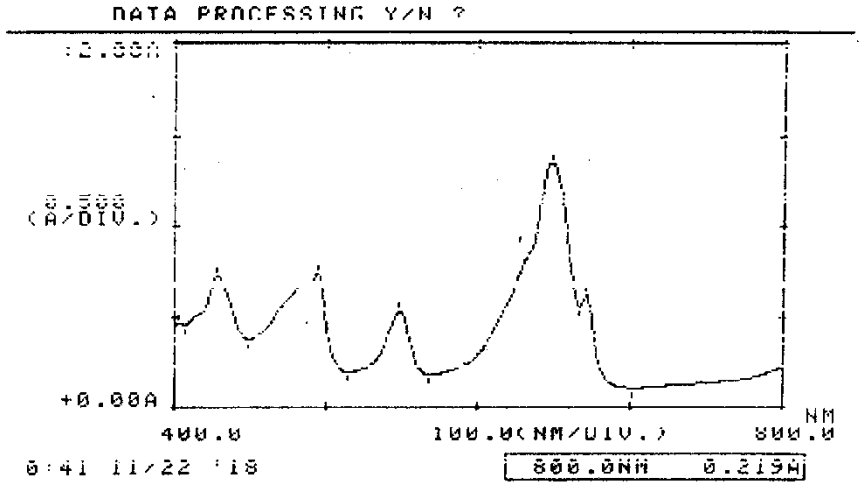

Fig-2: Spectra of 0.05 M U(IV) in 0.1 M HCl.

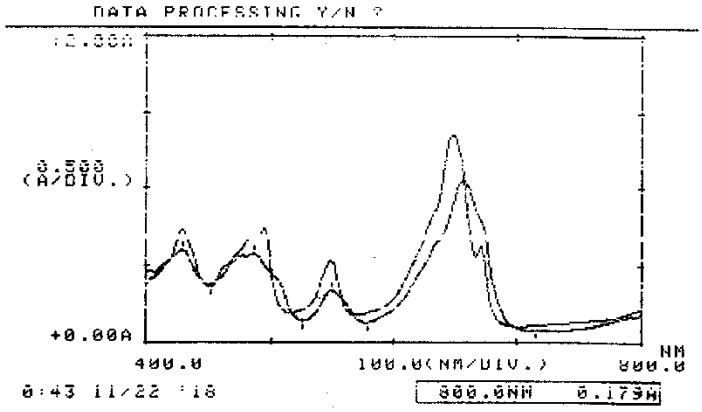

Fig-3: Spectra of 0.05 M U(IV) at in 0.1 M HCl and 0.03 M $[U(IV)\ HEDTA]^{1+}$ of at pH 3.0 and 0.1 M ionic strength.

Table-3: Effect of pH on psuedo first order rate constant k_{obs} for the reaction between $[U(IV)\ HEDTA]^{1+}$ and $[Fe\ (opt)_3]^{3+}$

Serial No.	pH	$10^2\ k_{obs}$ / s^{-1}
1	3.2	6.82 ± 0.23
2	3.0	11.21 ± 0.23
3	2.8	19.52 ± 0.24
4	2.5	32.12 ± 0.31

$[Fe\ (opt)_3]^{3+} = 3.0 \times 10^{-5}$ mol/dm^3 , Temperature = 30 °C
$[U\ (IV)\ HEDTA]^{1+} = 6.0 \times 10^{-4}$ mol/dm^3, μ = 0.01 mol/dm^3

Table-4: Effect of pH on second order rate constant k_1 for the reaction between $[U(IV)\ HEDTA]^{1+}$ and $[Fe\ (opt)_3]^{3+}$

Serial No.	pH	k_1 / $mol^{-1}dm^3\ s^{-1}$
1	3.2	111.8 ± 3.7
2	3.0	193.7 ± 4.7
3	2.8	344.7 ± 5.2
4	2.5	478.93 ± 4.9

$[Fe\ (opt)_3]^{3+} = 3.0 \times 10^{-5}$ mol/dm^3, Temperature = 30 °C
$[U\ (IV)\ HEDTA]^{1+} = 6.0 \times 10^{-4} - 11.0 \times 10^{-4}$ mol/dm^3

Table-5: Effect of ionic strength on psuedo first order rate constant $k_{obs.}$ for the reaction between $[U(IV)\ HEDTA]^{1+}$ and $[Fe\ (opt)_3]^{3+}$

Serial No.	Ionic strength mol /dm^3	$10^2\ k_{obs}$ / s^{-1}
1	0.01	11.91 ± 0.31
2	0.02	18.91 ± 0.34
3	0.03	22.48 ± 0.30
4	0.04	26.8 ± 0.33
5	0.05	30.1 ± 0.32

$[Fe\ (opt)_3]^{3+} = 3.0 \times 10^{-5}$ mol/dm^3, Temperature = 30 °C
$[U\ (IV)\ HEDTA]^{1+} = 6.0 \times 10^{-4}$ mol/dm^3, pH = 3.0

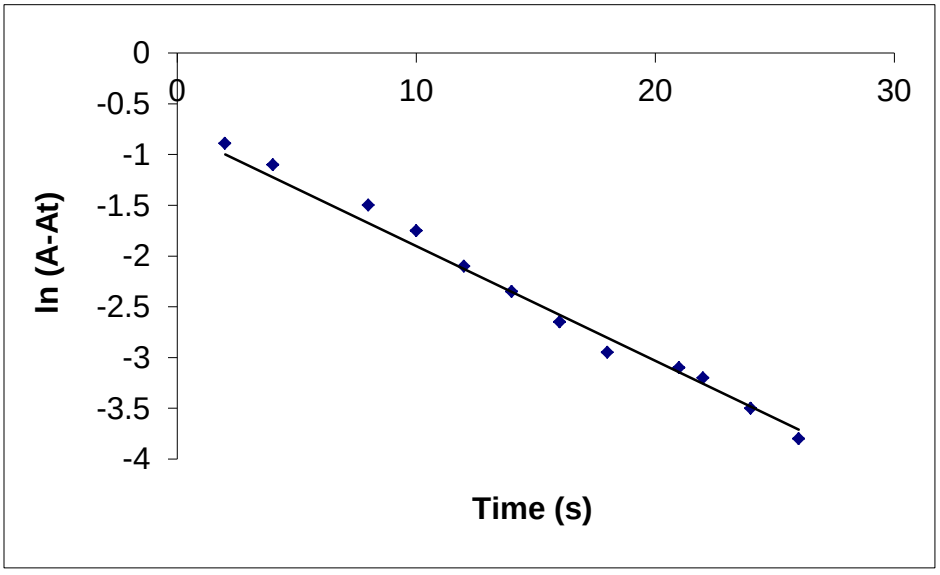

Fig-4 A typical kinetic plot for the determination of psuedo first order rate constant k_{obs} for the reaction between $[U(IV)HEDTA]^{1+}$ and $[Fe\ (opt)_3]^{3+}$.

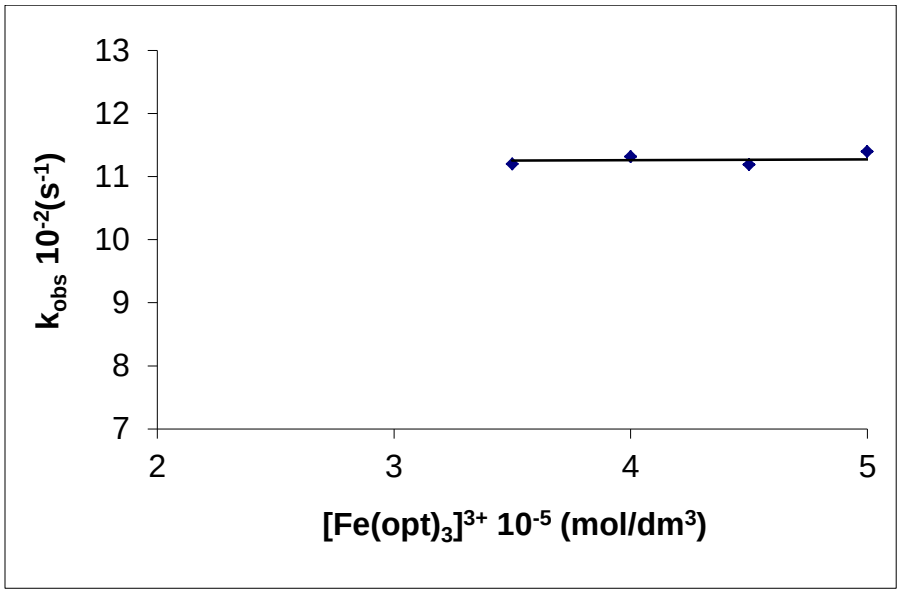

Fig-5: Effect of $[Fe(opt)_3]^{3+}$ on psuedo first order rate constant k_{obs} for the reaction between $[U(IV)HEDTA]^{1+}$ and $[Fe(opt)_3]^{3+}$.

Table-6: Effect of temperature on second order rate constant k_1 for the reaction between $[U(IV)\ HEDTA]^{1+}$ and $[Fe(opt)_3]^{3+}$

Serial No.	Temperature / °C	Number of replicates	$10^2\ k_{obs}$ / s^{-1}	k_1 / $mol^{-1}\ dm^3\ s^{-1}$
1	10	3	6.84	114.1 ± 3.2
2	15	3	8.29	138.3 ± 4.1
3	20	3	9.6	160.6 ± 3.9
4	25	3	10.2	170.5 ± 4.8
5	30	3	11.2	193.1 ± 4.2
6	35	3	17.26	288.1 ± 4.7

$[Fe(opt)_3]^{3+}$ = 3.0×10^{-5} mol/dm³, pH = 3.0
$[U(IV)HEDTA]^{1+}$ = 6.0×10^{-3} mol/dm³, μ = 0.01 mol/dm³

Table-7: Thermodynamic parameters for the reaction between $[U(IV)\ HEDTA]^{1+}$ and $[Fe(opt)_3]^{3+}$

$\Delta H^{\#}$ / kJ/mol	$\Delta S^{\#}$ / J/mol	$\Delta G^{\#}$/ kJ/mol	E_a / kJ/mol	ΔG° / kJ/ mol
15.3 ± 0.8	-150.6 ± 2	60.8 ± 1	19.31 ± 0.8	-30.6

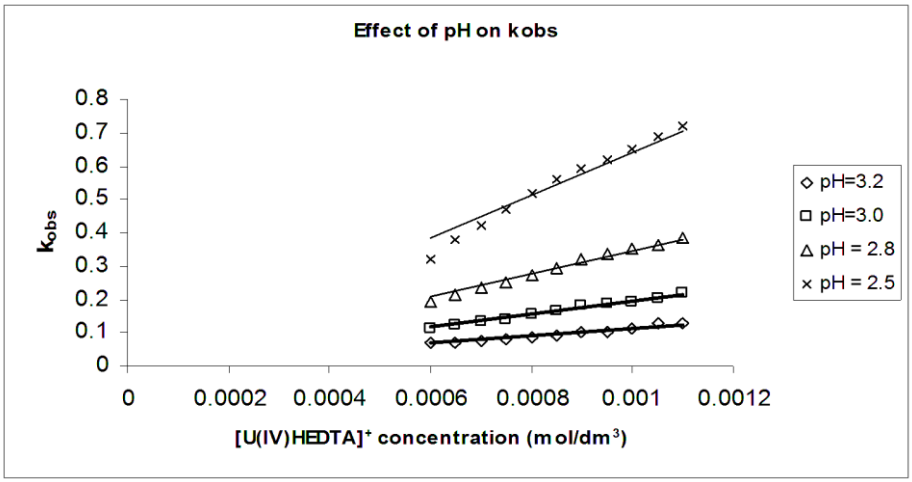

Fig-6: Effect of $[U(IV)HEDTA]^{1+}$ concentration on psuedo order first rate constant k_{obs} for the reaction between $[U(IV)HEDTA]^{1+}$ and $[Fe(opt)_3]^{3+}$.

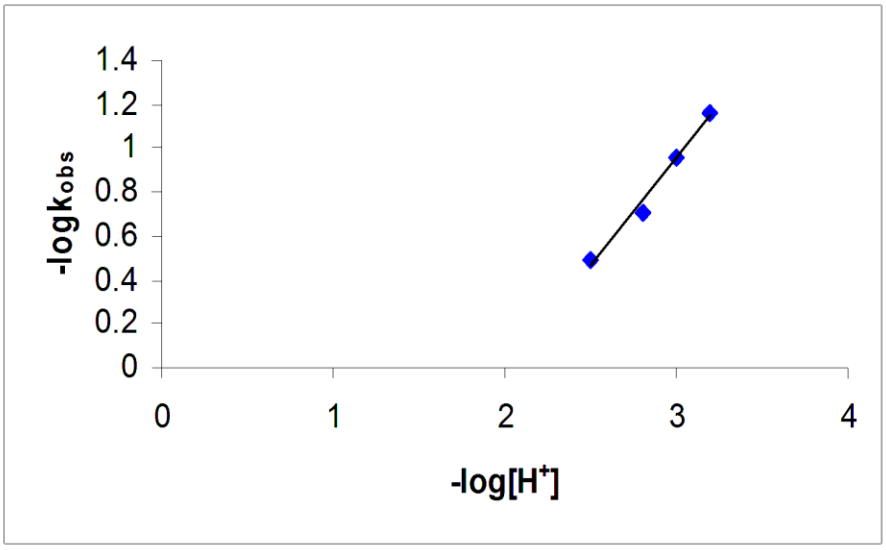

Fig-7: Effect of hydrogen ion concentration on second order rate constant k_1 for the reaction between $[U(IV)HEDTA]^{1+}$ and $[Fe(opt)_3]^{3+}$

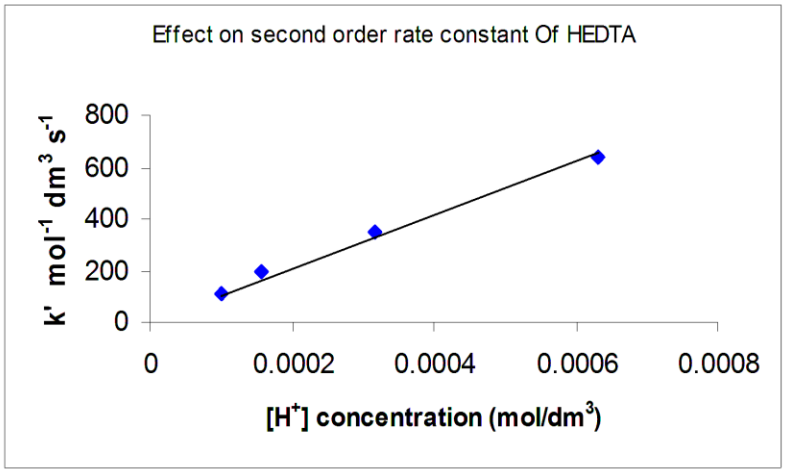

Fig-8 Effect of hydrogen ion concentration on second order rate constant k_1 for the reaction between $[U(IV)HEDTA]^{1+}$ and $[Fe(opt)_3]^{3+}$

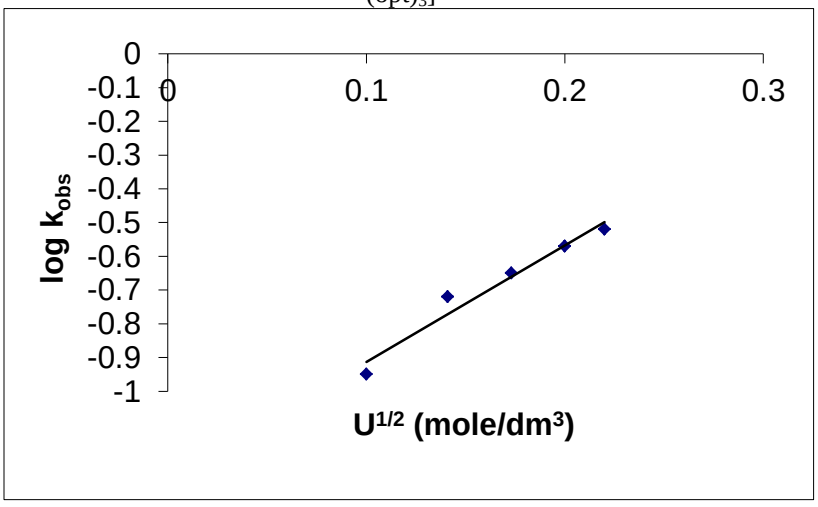

Fig-9: Effect of ionic strength on pseudo first order rate constant k_{obs} for the reaction between $[U(IV)HEDTA]^{1+}$ and $[Fe(opt)_3]^{3+}$.

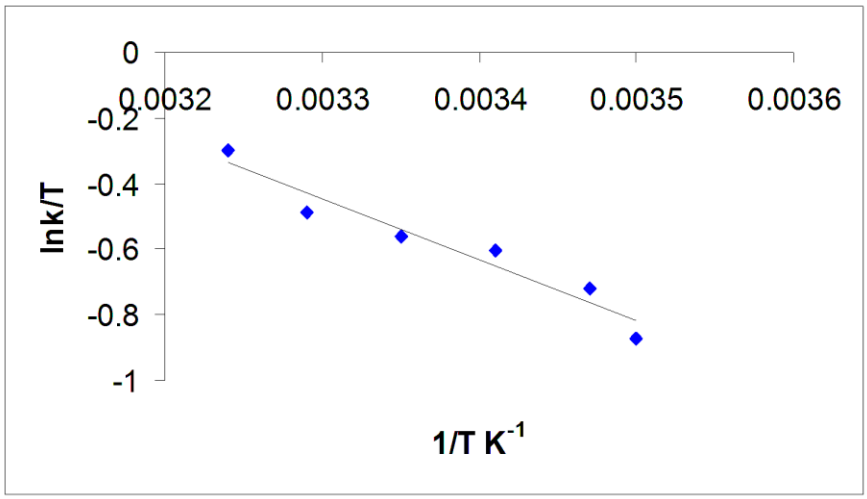

Fig-10: Effect of temperature to determine the thermodynamic parameters for the reaction between $[U(IV)HEDTA]^{1+}$ and $[Fe(opt)_3]^{3+}$

4. REFERENCES

1 Mudring, A.V. and Tang, S. Eur. J. Inorg. Chem. (**2010)** 569.
2 Girihar, P.; Venkatesan, K. A.; Srinivasan, T. G.; Vasudeva Rao, P. R. Electrochim. Acta (200752, 3006).
3 Ikeda, Y.; Hiroe, K.; Asanuma, N.; Shirai, A. *J. Nucl. Sci. Technol.* **(2009),** *46*, 158.
4 Hummel, W. Puigdomenech, I. ; Rao, L.; Tochiyama, O.; Chimie**,** C. R. **(2009),** 10**,** 948.
5 Hay, P. J. and Martin, R. L. Computational Studies of Actinide Chemistry, *Los* Alamos Science Number 26 (**2000**)
6 Thomson, R.K.; Graves, C.R.; Scott, B.L.; Kiplinger, J.L. *Dalton Trans*. **(2010),** 29 6826.
7 Antunes, M.A.; Dias, M.; Monteiro, B.; Domingos, A. and Santos, I. C. *Dalton Trans*., **(2006),** 3368.
8 Brandel, V.; Dacheux, N. and Genet, M. *J. Solid State Chem*., **(1996),** 121**,** 467.
9 Carey, G.H. and Martell, A.E. *J. Am. Chem. Soc*., **(1968),** 90, 32.
10 Salmon; Thue´ry, P. and Ephritikhine M. *Polyhedron*, **(2006),** 25, 1537.
11 Berthet, J.C.; Thuéry, Ephritikhine, M. *Inorg Chem*. **(2010),** 6; 49(17):8173-7.
12 Tanner, P.; Hung, S.T.; Mak, T. C. W.; Wang, R.J. *ChemInform*, **(1992),** 23, 21.
13 Charpin, P.; Folcher, G.; Nierlich, M.; Lance, M.; Vigner, D.; Navaza A. and Rango, C. de *Acta Cryst.* **(1990),** 46, 1778.
14 Antunes, M. A.; Dias, M.; Monteiro, B.; Aˆ ngela Domingos, Santos, I. C. And No´emia Marques, *Dalton Trans*., **(2006)**, 3368.
15 Fujii, S.; Tsue, C.; Yambe, K.; Nakjima, K. and Sakai, H. *Inorg. Chim. Acta*., **(2008)** 361**,** 1207.
16 Zang, V. and Eldik, R. V. *Inorg. Chem*., **(1990), 29**, 1705.
17 Shoukry, M.M.; Shehata, M. R.; Hamza, M.S.; Eldik van. R.; *Dalton Trans.* **(2005), 21**, 3921.
18 Luzzatto, E.; Cohen, H.; Stockheim, C.; Wieghardt, K.; Meyerstein, D. *Free Radic Res.* **(1995),** 23, 453.
19 Tzou, Y W.; Wang, M .K. and Loeppert, R.H. Chemosphere. **(2003),** 51**,** 993.
20 Tzou, Y.M.; Loeppert, R.H. and Wang, M.K. *Soil Science*. **(2002),** 167**,**729.
21 Abdel-Khalek, A.A.; Khalil, M.M. and Khaled, E. S. H. *J. Trans. Metal*, **(1993),** 18,153.
22 Naik, R.M.; Sarkar, J.; Chaturvedi, D.D.; Verma, A.; Singh, S.K. *Indian J. Chem. Sec. 42A*, **(2003),** 1639.
23 Luzzatto, E.; Cohen, H.; Stockheim, C.; Wieghardt, K.; Meyerstein, D. *Free Radic Res.* **(1995),** 23-453-63.
24 Carey, G.H. and Martell, A.E. *J. Am. Chem. Soc*., **(1968),** 90**,** 32.
25 Naqvi, S. I.I.; Farrukh, M. A and Qadri, M. M. *J. Chem. Soc. Pak.*, **(2002),** 24, 21.
26 Perveen, R. and Naqvi, I.I. *The Nucleus*, (**2004)** 41**,** 1.
27 Perveen, R. and Naqvi, I.I. *J. Saudi Chem.Soc*., **(2005),** 9,535.
28 Sutin, N. and Gordon, B.M. *J. Am. Chem. Soc*., **(1963),** 83**,** 70.
29 Naqvi, S.I.I. *J. Pak. Chem. Soc*., **(1980),** 2**,** 35.
30 Nelson. F., Kraus K. A. *J. Am. Chem. Soc.*, **(1951)**, 73, 2157.
31 Reagor, B.T. and D.H. Huchital. Inorg. Chem. **(1983),** 21**,** 703.
32 Seaman, G. C. and Haim, A.H. J. Am. Chem. Soc., **(1948),** 106**,** 1319.

Pak. J. Chem. 1(4):185-189, 2011 Full Paper
ISSN (Print): 2220-2625
ISSN (Online): 2222-307X

Measurement of dissolved hydrogen in Al alloys and calculation of hydrogen removal efficiency of a degassing system

[*]N. Akhtar, S. Javed and [1]W. Akhtar
[*]SOAN Enterprises Islamabad, Pakistan
[1]Department of Chemistry, University of Wah, Pakistan
E-mail: [*]naveed.so@gmail.com

ABSTRACT
In this paper we reported the diminution pattern of hydrogen contents in molten aluminium alloys during casting on industrial scale, and estimated the efficiency of inline rotary degassing system. The degassing parameters were tried to set constant in nearly 150 heats, so that other factors which govern the degassing efficiency of inline unit could be in-sighted well. In this study we used Leco RHEN-602 hydrogen determinator based on the principle of hot extraction carrier gas method, for the measurement of dissolved hydrogen in molten metal and from these results efficiency of inline rotary degassing unit was calculated. The results obtained were cross checked by observing hydrogen porosity in final castings; it endorsed the values obtained through RHEN-602 analyzer. This study showed that hydrogen removal efficiency of the rotary degassing unit was nearly 40 % for various aluminum alloys.

Keywords: Degassing, hydrogen contents, molten metal, porosity, removal efficiency.

1. INTRODUCTION
Hydrogen is the only gas that is appreciably soluble in molten aluminum and its alloys[1-3]. The solubility of hydrogen in aluminum increases rapidly with increasing temperature[1].Hydrogen in the liquid melt may arise from a number of sources i.e. disassociation of atmospheric moisture, products of combustion in gas fired furnaces, dissolved hydrogen in raw materials, moisture contamination of fluxes, incompletely dried furnace refractory and contamination from tools, flux tubes, ladles etc. Liquid aluminium has much larger solubility for hydrogen than solid aluminium, as a result during casting process hydrogen is released from the melt, creating pores in cast products. Although majority of the hydrogen is released, a small percentage may get trapped, creating hydrogen filled voids. This remaining hydrogen gas is the root cause of numerous failure mechanisms in aluminum products. Some authors[4-6] have reported the reduced mechanical properties and lower corrosion resistance due to hydrogen porosity.

The assimilation of hydrogen can be minimized by proper melting techniques[7], whereas dissolved hydrogen could be removed from the melt before casting by means of several techniques[8-12]. Degassing is the most common and effective way of reducing porosity due to hydrogen. Degassing methods utilizes chemically pure and dry gases; the most common are argon and nitrogen. The second one is cheaper and used most often for degassing purpose. Mixtures of reactive gases such as chlorine with nitrogen are also used and aid in cleaning the melt from inclusions[13-14]. During degassing bubbling of argon or nitrogen is done by means of a degassing rotor, which reduces the bubble size and disperses the carrier gas throughout the molten metal bath. As the carrier gas bubbles rise through the mass of molten metal they absorb the dissolved hydrogen and remove it from the melt. The efficiency with which the hydrogen is removed is directly related to the bubble size and gas dispersion within the melt[15-16]. It is a costly process so precise knowledge of the hydrogen content in the melt before and during degassing process is highly desirable. A number of techniques have been emerged to measure the degassing efficiency .i.e. reduced pressure test, electrochemical hydrogen sensor etc. In Pakistan peoples never choose a number of equipments for a similar purpose, for example in the presence of a laboratory type hydrogen analyzer they don't spend money on probe type analyzer. Therefore in this study we have employed the Leco hydrogen determinator (which analyzes solid samples only) for the estimation of degassing efficiency. We calculated the degassing efficiency from the hydrogen contents of holding furnace samples and hydrogen contents at casting station as follow;

$$\text{Efficiency} = (C_{H.Furnace} - C_{\text{Casting Station}})/C_{H.Furnace}$$

Where $C_{H.Furnace}$ and $C_{\text{Casting Station}}$ are the respective concentrations of the hydrogen gas before and after the degassing treatment.

2. EXPERIMENTAL

2.1 *Sampling and Sample Preparation*
Sampling of molten metal was done using a cylindrical copper mold to minimize the formation of voids. Sampling spoon and the mold was preheated before sampling of molten metal. After collection the sample was cooled instantly with cold

*Corresponding Author Received 25th August 2011, Accepted 6th September 2011

water. Solid samples were machined to get a uniform dimension of 10 x 24 mm. Sample size & weight, speed of lathe machine and other parameters were followed as described in Leco application notes[17-18]. After machining, the samples were washed with AR grade acetone and dried in warm air. All the prepared samples were handled with clean tweezers and analyzed quickly to minimize the surface contaminations.

Two samples from holding furnace before the melt moved into the degassing unit and two samples from casting launder after the degassing process were collected for the estimation of removal efficiency.

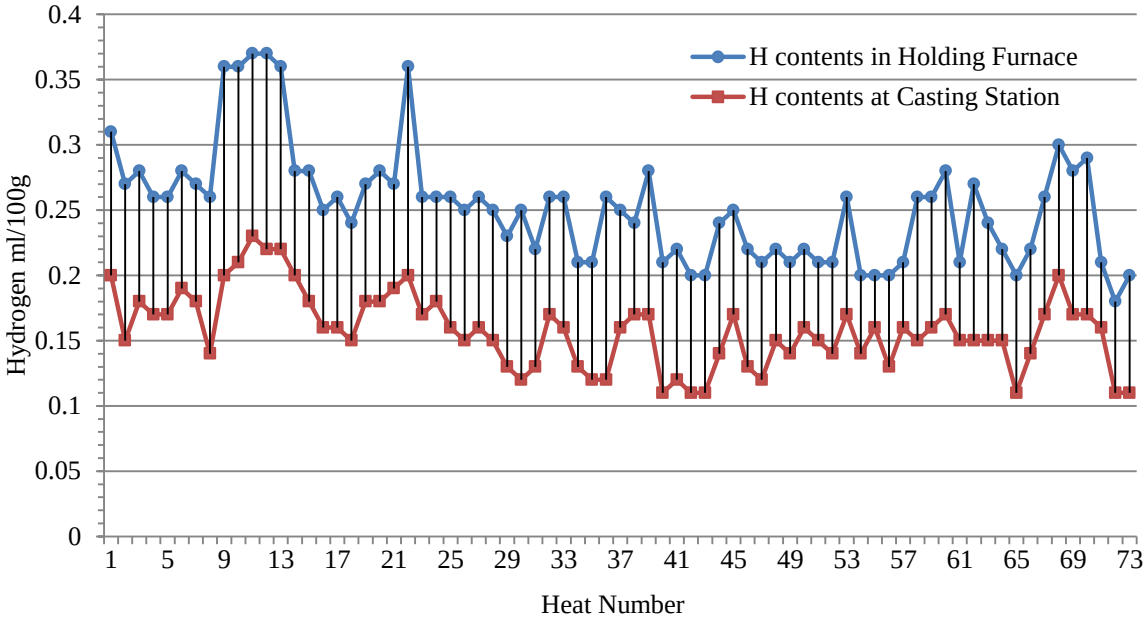

Fig-1: Hydrogen diminution pattern in 6xxx

2.2 *Method and Equipment*

Hydrogen gas continents in Al alloys samples were determined according to the standard procedures described in literature[17-19]. The equipment used was Leco hydrogen determinator RHEN-602.The working principle of this machine is based on the fusion of a sample in graphite crucible at a temperature above the melting point of that substance in an inert gas such as argon. Subsequently the thermal conductivity technique is utilized for the measurement of evolved hydrogen. The equipment was calibrated by reference standard materials provided by Leco, and drift was checked and corrected at regular intervals. The read out from equipment was in ppm unit and in % value by weight; the results were converted into ml/100g units purposefully for comparison with available literature.

2.3 *Macro etching of cast samples*

Hydrogen porosity test was conducted on casting logs of each heat. A 20 mm slice of the cast log along the cross section was taken and soaked in 10% NaOH solution for about 10 minutes. After washing the sample with tape water it was immersed in 10% HNO_3 for 5 minutes and then washed with water and dried in hot air. All the etched samples were checked for hydrogen porosity/ pin holes with magnifying glass and under the stereomicroscope.

3. RESULTS AND DISCUSSION

The results of molten metal samples before and after the degassing system have been plotted in Figure 1 to Figure 6. The upper curve having circle dots represents the hydrogen value as H_2 ml/100g Al in samples taken from holding furnace just before feeding the molten metal to rotary degassing unit. The lower curve having square dots represents the hydrogen concentration in molten metal after the degassing process. The drop line which connects the upper and lower points, represents the actual decrease as ml/100 g, from this value we have calculated the % efficiency of the degassing unit.

3.1 *Hydrogen contents of AA 6xxx*

Under 6xxx series 6011, 6061 and 6063 alloys were studied, hydrogen contents in the holding furnace ranged 0.18 minimum to 0.37 maximum. The average value in 73 heats was found 0.25 ml/100 g. It is notable that most of the high values in holding furnace samples are on the left side of the graph. Some of the values even crossed the 0.35 line; heat number 9 to 13 and heat number 22 showed maximum H_2 values. While investigating it was revealed that higher moisture levels of atmosphere around the holding furnace significantly contributed and raised the hydrogen contents of the molten metal. The results of samples collected just before casting demonstrated the actual decrease in dissolved hydrogen

contents while passing through the degassing unit. Hydrogen concentration in liquid metal after degassing treatment was found as low as 0.11 ml/100 g. The average hydrogen value in casting samples of 6xxx remained at 0.16 ml/100 g. The removal efficiency of rotary degassing unit ranged from a minimum 20% to 53.8% maximum in alloys of 6xxx series (Fig-6).

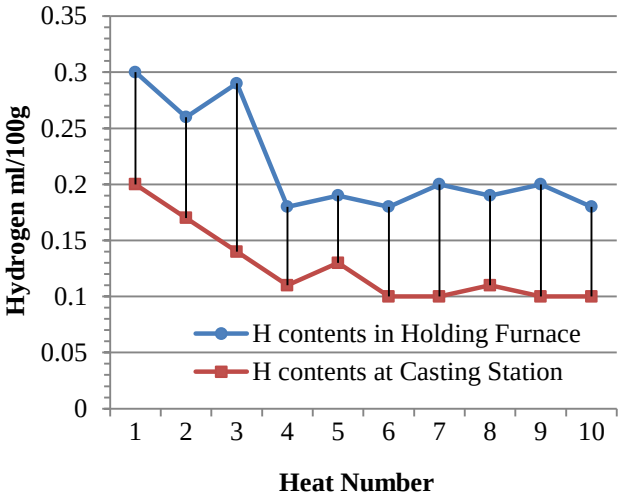

Fig-2: Hydrogen diminution pattern in 5xxx

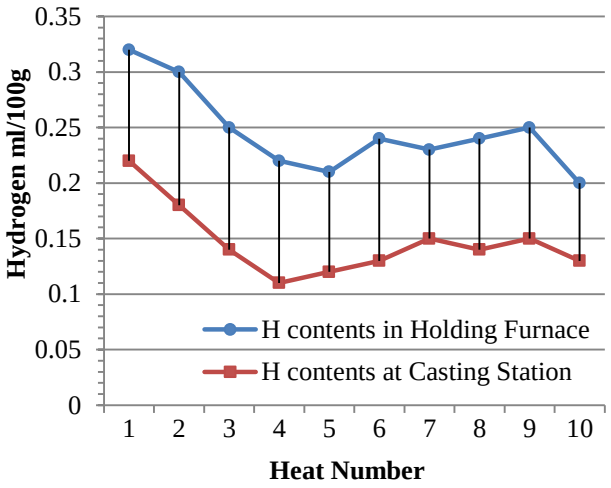

Fig-3: Hydrogen diminution pattern in 3xxx

3.2 *Hydrogen contents of AA 5xxx*

The main alloys of 5xxx series casted during this study were 5050, 5052 and 5083. Hydrogen concentration varied in holding furnace samples from 0.18 – 0.30 ml/100g with an average value of 0.22 ml/100 g. It was observed that whenever greater quantities of scrap metal was used in the manufacturing of alloy, greater hydrogen contents were found in the holding furnace samples i.e. melting number 1, 2 and 3 utilized 20-30% in-house scrape (Fig. 2). Molten metal samples collected after degassing ranged 0.10 -0.20 with an average of 0.13 ml/100g. The maximum decrease was observed in melting number 3 and it was 51.7% as shown in Fig-6.

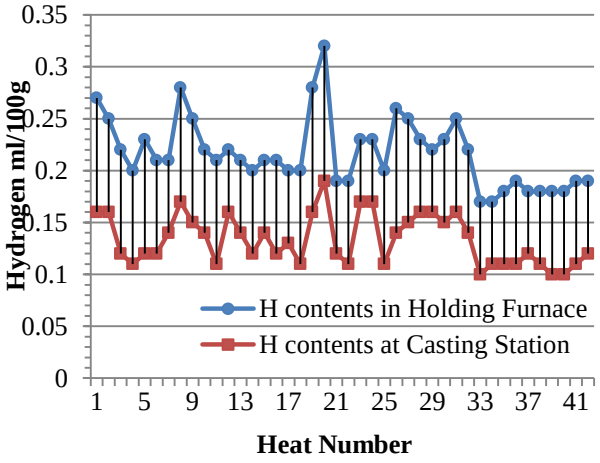

Fig-4: Hydrogen diminution pattern in 2xxx

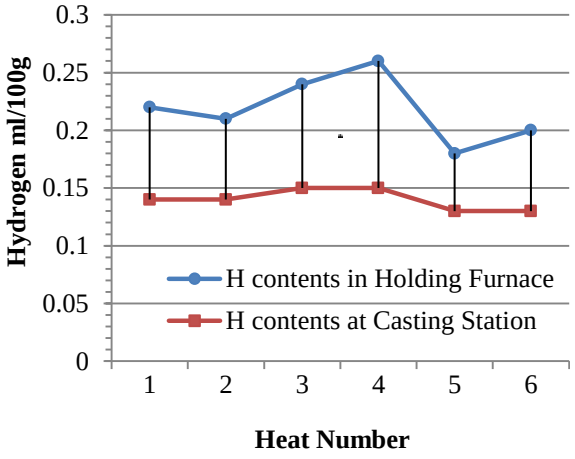

Fig-5: Hydrogen diminution pattern in 1xxx

3.3 *Hydrogen contents of AA 3xxx*

The graph of 3xxx series looks like a perfect ladder (Fig. 3), average decrease in hydrogen value was found 0.1 ml/100g while moving from holding furnace to casting station through rotary degassing unit. The removal efficiency varied in the range of 31.3% minimum to 50% maximum (Fig. 6).Hydrogen contents at casting station were below 0.15 ml/100g in most of the heats, which is a minimum requirement for good quality castings.

3.4 *Hydrogen contents of AA 2xxx*

The 2xxx series under study comprised of 2014, 2018, 2024, 2036, 2050, 2219 and 2618 alloys. Hydrogen concentration in holding furnace ranged 0.17 -0.32 with an average of 0.22 ml/100 g (Fig-4). The highest values were observed in the rainy season when the moisture in air was high. After degassing average H_2 value obtained was 0.13 with a minimum 0.10 and a maximum 0.19 ml/100g in samples collected from casting launder just before casting. Average removal efficiency of degassing unit was lingered at 38.6% (Fig-6).

3.5 *Hydrogen contents of AA 1xxx*

In 1xxx series 1050 alloy was casted during this study; from fig. 5 it is noticeable that there is no elevated reading in holding furnace samples, H_2 values remained below the 0.30 barrier. But on the other hand neither of the casting samples came down to 0.1 ml/100g level, in fact all samples after degassing hang around 0.15 ml/100g value. We observed 35.4% average hydrogen removal efficiency of the degassing unit for 1xxx (Fig-6).

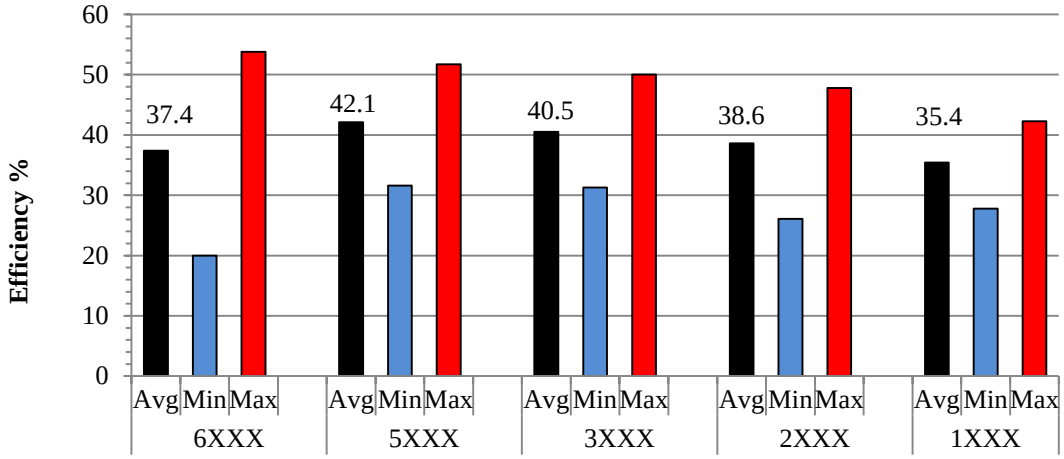

Fig-6: Hydrogen removal efficiency of inline rotary degassing system for various Al alloys

3.6 *Hydrogen removal efficiency*

The hydrogen removal efficiency of inline rotary degassing unit has been plotted in Fig. 6, which shows the minimum, maximum and average efficiency in various series of Al alloys under study. The removal efficiency ranged 20-53.8% with an average value of 38.4% in various aluminium alloys.

3.7 *Results of porosity test*

Porosity test showed that whenever the hydrogen gas exceeded the 0.17 ml/100g value in the molten metal samples from casting launder, the pin holes were seen in the casting log samples directly with naked eye or under magnifying glass. It was also observed that porosity due to hydrogen was more prominent towards the periphery of the cast log sample. All the heats which contained H_2 less than 0.15 ml/100g at casting station showed no such problems and produced good quality castings. This test also confirmed the quantitative readings obtained from Leco RHEN-602 determinator.

4. CONCULSIONS

The absorption and accumulation of hydrogen gas in molten metal depends upon the raw materials, scrap %age and humidity level along with some other factors like natural gas purity etc. This study proved that Leco hydrogen determinator RHEN-602 can be used effectively for the detection of hydrogen contents in molten metal, and for the estimation of degassing efficiency. The average hydrogen removal efficiency of inline rotary degassing unit under study was lingered at 40%. Porosity test showed that H_2 values above 0.15 ml/100g in molten metal at casting station can cause serious damage to final castings.

5. ACKNOWLEDGEMENT

The authors are deeply indebted to Ms. Nosheen and Ms. Mobeen Ibad for their assistance during the preparation of manuscript and proof reading.

6. REFERENCES

1. G. D. Alternpohl; *Aluminium technology*, 6th edition, TMS-AIME, warrendale, PA, **(1998)**, p.61.
2. J. R. Scully, G.A. Young and S.W. Smith; *Materials Science Forum*, **(2000)**, 331-337, 1583-1600.
3. D. E. J. Talbot; *International Metallurgical Reviews*, **(1975)**, 20, 166-184.
4. P. J. Ferreira, I.M. Robertson and H.K. Birnbaum; *Acta Mater*, **(1999)**, 47, 2991-2998.
5. G. Laslaz and P. Laty; *AFS Transactions*, **(1991)**, 99, 83-90.
6. G. M. Bond, I.M. Robertson and H.K. Birnbaum; *ActaMetall*, **(1988)**, 36, 2193-2197.
7. S. Shivkumar, L. Wang and D. Apelian; *JOM*, **(1991)**, 43, 26-32.
8. H. Puga, J. Barbosa, E. Seabra, S. Ribeiro and M. Prokic; *AES-ATEMA Fourth International Conference*, Hamburg, **(2009)**.
9. M. Makhlouf, L. Wang and D. Apelian; Hydrogen in aluminum alloys-Its measurement and its removal, a monograph published by AFS, Des Plaines, IL, **(1998)**.
10. F. Moldovan, I. Chira and M. Pana; *Journal De Physique*, **(1993)**, 3, 747-754.
11. Y. Ohn; *Journal of Japan Institute of Light Metals*, **(2001)**, 51, 134-137.
12. R. R. Corns and T.P. Rack; *AFS Transactions*, **(1989)**, 97, 983-988.
13. G. K. Sigworth; *AFS Transactions*, **(1987)**, 95, 73-78.
14. G. K. Sigworth; *Light Metals*, TMS, **(1999)**,p.641.
15. G. K. Sigworth and T.A. Engh; *Metallurgical and Materials Transactions*, **(1982)**, 13, 447-460.
16. J. G. Stevens and H. Yu; *Light Metals*, **(1988)**, pp.437-443.
17. http://www.leco.com/resources/application_note_subs/pdf/inorganic/Analytical%20Tips/O-N-HDetermination209-141-004.pdf
18. http://www.leco.com/resources/application_note_subs/pdf/inorganic/-300.pdf
19. Annual Book of ASTM Standards, Vol. 3.05, ASTM, Pennsylvania, **(2001)**, pp.903–905.

Pak. J. Chem. 1(4):190-192, 2011 Full Paper
ISSN (Print): 2220-2625
ISSN (Online): 2222-307X

Estimation of Moisture Content & Metal Ions in White Flowers of *Bougainvillea spectabilis* and Purple Flowers of *Bougainvillea glabra* in Pakistan

[*]S. A. Rashid, F.S. Rehmani, [1]M. Arman, M. Ibrahim and [2]S. Shafique,
[*]Department of Chemistry, University of Karachi, Pakistan,
[1]Pharmaceutical Research Centre, PCSIR. Laboratories Complex, Karachi-75280, Pakistan
[2]Liaquat College of Medicine and Dentistry and Darul Sehat Hospital, Karachi, Pakistan
E-mail: [*]asma_rashid40@yahoo.com

ABSTRACT

Bougainvillea consists of 18 shrubby species, growing in different parts of Pakistan and is being used as Anti-ulcer, Anti-diarrheal, Anti-microbial, Anti- diabetic, Amylase Inhibition and as for low blood pressure but none of the studies on Bougainvillea focused on the estimation of metal ion concentration. The focus of the present study was to estimation of moisture content and comparative analysis of trace metal ions in white flowers of *Bougainvillea spectabilis* Willd and Purple flowers of *Bougainvillea glabra* Choisy. The metal ions concentration either essential or non essential, critically affect the biological system of the human body. Here are many factors including the different types of pollution-fertilizer, insecticides, pesticides and other forms of air and water pollution etc.- that effect directly on metal ion concentration in *Bougainvillea* and indirectly in biological system if used traditionally as medicine.

Keywords: Bougainvillea white and purple flowers, Metal ions, Environmental effects, Health effects

1. INTRODUCTION

Nyctaginaceae is a family of 30 genera and about 290 species found in tropical and subtropical parts of both hemispheres, and especially America. This family is represented in Pakistan by five genera, one of which, *Bougainvillea*, consists of 18 shrubby species. *Bougainvillea* is a climbing shrub with spines and showy flowers, the color of which ranges from white, purple [Fig-1] yellow, orange, various shades of red & purple and violet[1].Biological and chemical reported data describes that *Bougainvillea* show evidence of variety of properties like, color and bioactivity [1]Anti-ulcer / Anti-diarrheal / Anti-microbia activity as leaves studied for anti diarrheal, anti-ulcer, and anti-microbial activities[2], Insulin-like effect of pinitol ,D-pinitol (3-O-methyl-chiroinositol) [Fig-2]an active principle of the traditional antidiabetic plant .*Bougainvillea spectabilis (*B. *spectabilis)*, is claimed to exert insulin-like effects. This study investigates the effect of D-pinitol on glucose homeostasis in animal models of diabetes, and on glucose transport by cultured muscle cells[3], Antimicbacterial, Antidiabetic, Amylase Inhibition such as study of the chloroform extract of *Bougainvillea spectabilis* showed significant alpha-amylase inhibitory property[4], Anti-fertility, Antihyperlipidemic / D-pinitol, radical scavenging activity found in the aqueous extracts of B. *spectabilis* produced more free radical scavenging than Bauhinia *divaricata*. Results were superior to common synthetic antioxidants used in the food industry and presents a potential for applications in pharmaceutical or alimentary preparations[5]. The alcoholic extract of leaves of *Bougainvillea* are more active against Gram positive and Gram negative bacteria[6]. An antiviral protein active against mechanical transmission of tomato spotted wilt virus was identified in the root tissues of *Bougainvillea spectabilis* Willd[7].Overall *Bougainvillea* is being used for a variety of disorders, for diarrhea, and to reduce stomach acidity elsewhere, for cough, sore throat, for blood vessels for hepatitis, a decoction In Panama, an infusion of the flowers of *Bougainvillea glabra* also used as treatment for low blood pressure.

A B

Fig-1: (A) White *Bougainvillea spectabilis* Willd (B) Purple *Bougainvillea glabra* Choisy
Origin: (Botanical garden of University of Karachi)

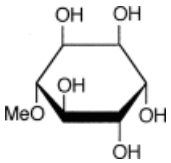

Fig-2: Structure of D-pinitol (1 D-3-O-methyl-chiroinositol).

*Corresponding Author Received 20th December 2011, Accepted 23rd December 2011

The ignorant people from other parts of the world and also those from Pakistan who are illiterate habitually use herbal extract for the cure of certain traditional diseases and exposed to large amount of toxic elements., such as Iron overload is a condition in which iron deposited in liver, kidney and spleen of human beings & instead of its importance iron could be toxic. When in excess, it damages the tissues[8].The aim of our study was to estimate the concentration of Ca, Na, K, Mg, Zn, Mn, Cu and Fe in white and purple flowers of *Bougainvillea* growing in Pakistan.

2. EXPERIMENTAL

Samples of *Bougainvillea* were collected in morning time and transported to the laboratory in polythene bags. The flower petals were dried in oven and grinded to powder form by using electrical grinder. All chemicals and standards used were of analytical grade. Metal ions analysis was carried out by AAnalyst 700 Atomic Absorption Spectrometer – (PerkinElmer).Moisture content determined by using lab grade oven.

2.1 *Determination of moisture content*

The fresh sample of flower , leaf and stem was selected for estimation of water content measurement .Initially weighed accurately 1 gm of each then dried to a constant mass in an oven at a temperature of 100°C.Final weight was recorded and % moisture calculated on the basis of fresh and dry masses in gm by using formula

$$\%\text{MOISTURE} = \frac{\text{Initial weight (gm)} - \text{Final weight (gm)}}{\text{Initial weight (gm)}} \times 100$$

2.2 *Estimation of metal ions in white and purple colored flowers*

One gm stored powdered sample of each white and purple colored flower , soaked separately in 25 ml of 1 N HCl for 24 hr, then filtered through filter paper Whatman no 42.Final volume was made up to 50 ml in volumetric flask by using ultra pure water .Ca, Na, K, Mg, , Zn, Mn, Cu & Fe were analyzed by the use of AAnalyst 700 Atomic Absorption Spectrometer – (PerkinElmer) .Absorbance values recorded at different wavelength precise for each metal ion. The calibration curves were constructed using a series of dilutions containing different levels of metal ions.

3. RESULTS AND DISCUSSION

It was observed, water content in purple flowers of *Bougainvillea glabra* choisy 79.46 %, in leaf 75.64% and in stem 69.17%. It was 81.68% in white flowers of *Bougainvillea spectabilis*, 72.35 % in leaf and 66.2 % in stem. In both white and purple colored flowers of *Bougainvillea* moisture % is in increasing order as stem < leaf < flower [Table 1,2 & Fig-3].Calibration curved were used for the determination of accurate values of metal ions in ppm. [Table-3] showed that In both purple and white flowers concentration of metal ions is in decreasing order as follows K > Mg > Fe > Na > Ca > Mn > Zn > Cu. Concentration of potassium is highest in both flowers (56.79 ppm) ,as K is highly mobile and can aid in balancing the anion charges within the plant. It also has high solubility in water and leaches out of soils that rocky or sandy that can result in potassium deficiency. Comparatively level of Potassium ions in both flowers are equivalent but Mg, Fe, Ca, Mn, and Zn is greater in purple flowers. Plants deficient in magnesium show stress responses. The first observable signs of both magnesium starvation and over exposure in plants is a decrease in the rate of photosynthesis. This is due to the central position of the Mg^{++} ion in the chlorophyll molecule means in plants, magnesium is necessary for synthesis of chlorophyll and photosynthesis. Iron is essential to nearly all known organisms such as for photosynthesis and is also present as an enzyme cofactor in plants. Calcium regulates transport of other nutrients into the plant and is also involved in the activation of certain plant enzymes. Calcium is one of the most important elements in the diet because it is a structural component of bones, teeth, and soft tissues and is essential in many of the body's metabolic processes. Manganese is necessary for building the chloroplasts. Manganese deficiency may result in coloration abnormalities, such as discolored spots on the foliage. Manganese is an essential trace nutrient in all forms of life. The classes of enzymes that have manganese cofactors are very broad and include oxidoreductases,transferases, hydrolases, lyases, isomerases, ligases,lectins, and integrins. Zinc is required in a large number of enzymes and plays an essential role in DNA transcription. Level of sodium is slightly greater in white (8.985 ppm) > purple (8.850 ppm) flowers. It can also substitute for potassium in some circumstances.

Table-1: Moisture content in flower , leaf and stem –*Bougainvillea glabra* Choisy, Purple

Bougainvillea Purple	Initial weight (gm)	Final weight (gm)	Difference (Initial-Final) (gm)	% Moisture
Flower	1.000 +/-0.001	0.2054	0.7946	79.46 +/-0.001
Leaf	1.000 +/-0.001	0.2436	0.7564	75.64+/-0.001
Stem	1.000 +/-0.001	0.3083	0.6917	69.17+/-0.001

Table-2: Moisture content in flower , leaf and stem –*Bougainvillea spectabilis* Willd, White

Bougainvillea White	Initial weight (gm)	Final weight (gm)	Difference (Initial-Final) (gm)	% Moisture
Flower	1.000 +/-0.001	0.1832	0.8168	81.68+/-0.001
Leaf	1.000 +/-0.001	0.2765	0.7235	72.35+/-0.001
Stem	1.000 +/-0.001	0.3379	0.6620	66.20+/-0.001

The ratio sodium/potassium concentrations in intercellular and extracellular fluids is responsible for the transport ions through the cellular membranes, the regulation of the osmotic pressure inside the cell, the transmission of nervous pulses and other electrophysiological functions. Concentration of copper is also less in purple (0.135) < white (0.160), Copper is required for the normal functioning of plants, animals, humans, and most microorganisms. It is incorporated into a variety of proteins which perform specific metabolic functions**.** The level of copper is least in both flowers and it is also needed in relatively small amounts which can be stored in the body, and daily presence in the diet is therefore not necessary.

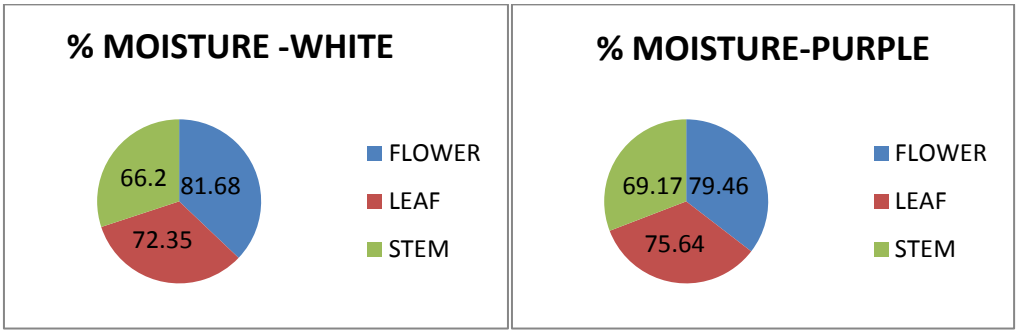

Fig-3: % moisture in flower, leaf & stem

Table-3: Concentration of metal ions in white & purple flowers

Wavelength (nm)	**422.7**	**589.0**	**766.5**	**285.2**	**213.9**	**279.5**	**324.8**	**248.3**
Analyte in Purple flower (ppm)	**Ca**	**Na**	**K**	**Mg**	**Zn**	**Mn**	**Cu**	**Fe**
Replicate No 1	5.719	8.888	56.79	30.88	0.334	0.585	0.134	26.98
Replicate No 2	5.699	8.835	56.79	29.86	0.336	0.584	0.133	26.56
Replicate No 3	5.779	8.828	56.79	29.07	0.326	0.589	0.136	26.82
Mean concentration (ppm)	5.732	8.850	56.79	29.94	0.332	0.586	0.135	26.78
SD	0.0417	0.0328	0.001	0.908	0.0054	0.0029	0.0015	0.214
% RSD	0.73	0.37	0.00	3.03	1.63	0.50	1.15	0.80
Analyte in White flower(ppm)	**Ca**	**Na**	**K**	**Mg**	**Zn**	**Mn**	**Cu**	**Fe**
Replicate No 1	2.468	8.916	56.79	24.65	0.251	0.469	0.161	10.37
Replicate No 2	2.463	8.990	56.79	25.75	0.245	0.474	0.160	10.52
Replicate No 3	2.485	8.970	56.79	24.75	0.248	0.473	0.160	10.39
Mean of concentration (ppm)	2.472	8.958	56.79	25.05	0.248	0.472	0.160	10.43
SD	0.0118	0.0385	0.002	0.606	0.0033	0.0028	0.0004	0.084
% RSD	0.48	0.43	0.00	2.42	1.34	0.59	0.27	0.81

SD = standard deviation, %RSD = percent relative standard deviation

4. CONCLUSION

The present investigation showed that the concentrations of different metals ions Mg, Fe, Ca, Mn, and Zn in white and purple flowers are not exactly same and further can be altered badly by the change in environmental conditions. Thus, in the light of our studies, the conclusion may be drawn that metal ions either deficient or in overload condition can causes severe effect in biological system as responsible for various chemical and biochemical imbalance.

5. ACKNOWLEDGEMENT

We are very thankful to Mr. Saleem & Ms. Kausar of the Department of Botany of University of Karachi for identifying the flowers.

6. REFERENCES

1. Ali,M. S.,Natural Product Research, **(2005)** 19: 1 - 5
2. Edwin,E; SheejaE;Toppo,E; Tiwari,V; KR Dutt. Ars Pharm, **(2007)** 48 (2): 135-144
3. Bates S. H; Jones R. B; Bailey C. J. / Br J Pharmacol. **(2000)** 130(8): 1944–1948
4. Bhat M, Zinjarde SS, Bhargava SY, Kumar AR, Joshi BN. Evid Based Complement Alternat Med. **(2008)**
5. Chaires-Martinez L et al / a Pharmacognosy Research **(2009)** 1(5).238- 244
6. Umamaheswari,A, Shreevidya,R and Aparna Nuni Advances in Biological Research **(2008)** 2 (1-2): 01-05
7. Balasaraswathi R, Sadasivam S, Ward M, Walker JM. Phytochemistry. **(1998)** 47(8):1561-5
8. Rehmani.F.S, Pakistan J. Saudi Chem. Soc., **(2005)** 9(2): 265-270
9. Rehmani.F.S, Journal of Chemical Society of Pakistan, **(2005)** 27(3):263-267
10. Rehmani.F.S Journal of Chemical Society of Pakistan **(2006)** 26(6):552-556
11. Rehmani.F.S Journal of the Chemical Society of Pakistan,**(2010)** 32 (4) 467-470
12. Azmat.R.; Saba Haider, Mreena Riazi, Pak. J. Bot., **(2009)** 41(5): 2289-2295
13. Azmat.R; Naila Khan, Pak. J. Bot. **(2011)** 43(1): 515-520
14. H. Saikia A. Lama , International Journal of Pharmaceutical Sciences and Drug Research **(2011)** 3(2): 141-145

Guide for Authors

Pakistan Journal of Chemistry is an international peer-reviewed journal published in English by a National Chemist Community of International Repute, with its editorial office hosted by the Department of Chemistry, University of Karachi, Karachi, Pakistan. It publishes original research and review work (either theoretical and applied) in all fields of chemistry, i.e. physical, inorganic, organic and analytic chemistry, computational, environmental, photochemistry, photobiology, organometallic synthesis, nanotechnology, medicinal and drug etc. in the forms of Accounts, Full Papers, Notes and Communications. The authors must inform the Editors of manuscripts submitted to, soon to be submitted to, or in press at other journals that have a bearing on the manuscript being submitted.

All submissions must be in keeping with the Ethical Guidelines to Publication of Chemical Research of the European Association of Chemical and Molecular Sciences. In particular, authors should reveal all sources of funding for the work presented in the manuscript and should declare any conflict of interest. Manuscripts containing animal experiments must include a statement in the Experimental Section to state that permission was obtained from the relevant national or local authorities. The institutional committees that have approved the experiments must be identified and the accreditation number of the laboratory or of the investigator given where applicable. If no such rules or permissions are in place in the country where the experiments were performed, then this must also be clearly stated. Manuscripts with experiments with human subjects or tissue samples from human subjects must contain a disclaimer in the Experimental Section to state that informed signed consent was obtained from either the patient or from next of kin. All articles must be written in English. Authors less familiar with the English language should seek assistance from proficient colleagues in order to produce grammatically and semantically correct manuscripts.

Each contribution submitted to the Pakistan Journal of Chemistry will be sent to independent referees. Authors are encouraged to suggest three (3) suitable referees from Europe and North America (full names and affiliations including E-mail address). However, not exclusively those referees nominated by the authors will be contacted. All accepted manuscripts are edited before printing to ensure scientific consistency, clarity of presentation, and uniformity of style.

For any assistance or query, please visit the website, or you can also email us.

Website: www.pjchm.com
Editor: editor@pjchm.com
Technical Editors: technical@pjchm.com

Journal is indexed in Chemical Abstract, Cab Abstract, Copernicus Index, DOAJ, and Google Scholar & under review in ISI Thomson Reuter and Scopus.
Note: All Papers must be submitted online.
Publication Cost (National / International): 3,000 Rs. / 100$ (USD)